Conductive atomic force microscopy measurements on organic nanocrystals

Master Thesis

by

Sven Renkert

Reviewer: Prof. Dr. Günter Reiter

Fakultät für Mathematik und Physik
Physikalisches Institut
Albert-Ludwigs-Universität Freiburg
Germany
September 2014

Contents

1. Motivation

Conjugated polymers were studied intensively in the last decades, because organic semi-conductors can be processed much easier and in the large scale (and thus more cost effective) than their inorganic counterparts. In addition, they are mechanically more flexible. They found important technical applications in optoelectronic devices such as light emitting diodes (LEDs), solar cells [1], and field-effect transistors (FETs) [2], each being a huge topic of research on its own. Despite its successes in applications, transport processes in organic semiconductors are yet not fully understood. It is well known that the molecular order plays a major role for charge transport properties. Here organic semi-conductor single crystals can serve as a model system to study transport mechanisms, as they provide a regular molecular ordering with a low concentration of charge traps [3]. Many different systems are studied intensively, e.g. rubrene, polythiophene and polyacety-lene. Even though organic semiconductors have many advantages, partly since they up to date, they only reach or overcome the performance of inorganic semiconductors in special situations as such as low temperature or if mechanical flexibility is a necessary feature. In the last decades, the performance was increased by orders of magnitude, overcoming the mobility of amorphous silicon [4]. Understanding the key transport mechanisms will even-tually improve the performance of these devices even further. In addition, understanding the relationship between macroscopic properties and microscopic properties, concerning both chemical structure and secondary order, is a necessary knowledge to master chem-ical engineering. A proper understanding of chemical engineering will consequently lead to high performances of molecules designed with this knowledge.

The aim of this thesis is to study the charge transport properties of a newly synthe-sised family of conjugated molecules, commonly called TBT. The oligomer is chemically designed to enhance supramolecular charge transport in its crystalline state. This can be achieved through π-π-interactions between the end thiophene rings of neighbouring molecules. The conjugated backbone of this molecule is designed to be rather rigid, in or-der to enhance crystallisation and to enable close π-stacking at the same time. Sidechains are attached to the molecules to make them easily solvable in various organic solvents.

Thus the processing is easier and better controllable, and the molecules can be crystallised out of solution.

Up to date, major approaches to measure the electron mobility of organic semiconductor single crystals are e.g. transmission line measurements [5], four-probe measurements [6] and time of flight measurements [7]. Whereby transmission line and four-probe measurements need macroscopic contacts with their respective contact resistances. Although the contact resistances can be calculated in principle, and thus separated from the resistance of the organic field effect transistor devices with these techniques, in many cases it is a much more complex problem and can not be solved easily. In addition, applying a macroscopic contact to for example a rubrene single-crystal has been shown to introduce defects into the crystal [8]. Rarely the conductive atomic force microscope (C-AFM) is used to investigate the charge transport properties [9]. This thesis aimed at a better understanding of C-AFM measurements on organic semiconductor single crystals, focussing on 3TBT. One of the advantages of C-AFM over, for example, transmission line measurements lies in the reduction of contact effects when measuring I-V-spectra. The tip position and the interaction between tip and sample can be controlled directly by AFM, circumventing the problems of macroscopic contacts. Therefore, C-AFM could close this gap and enable measurement on pristine crystals.

During the experiments, the focus of the thesis changed, since some of the crystals turned out to be mechanically unstable when measuring with AFM in contact mode. As long as these instabilities were not fully understood, performing C-AFM measurements was not allowing to obtain reliable results. First of all, taking I-V-characteristics with tips that might have been damaged in earlier measurements, when breaking crystals in an unknown fashion, is not a valuable scientific approach. Secondly, choosing only the crystals that were stable could introduce a bias in the data, as long as the reason for mechanical instabilities is not understood. Lastly, such an approach introduces unbearably time consuming search for suitable crystals. Therefore the main interest of the experiments in this study lies on the investigation of mechanical stability of 3TBT crystals. As we will show, we now understand the mechanical instabilities, thus having prepared the investigation of TBT-crystals with C-AFM. The research may also be helpful for the future investigation of other organic crystals. In addition, we are able to manipulate and cut the crystals on the macroscopic scale in a controlled manner.

2. Theoretical Background

This chapter first gives a brief introduction to atomic force microscopy (AFM) in general, with a focus on its properties specifically relevant to understanding the experiments performed in this study. A comparison between conductive AFM and other methods to measure the mobility of semiconductors is given. Then we describe common methods of crystallisation (for organic semiconductors) and the chemical design of the TBT family, the organic oligomer we investigate in this study. Besides that we integrate the thesis into the context of previous studies.

2.1. Atomic Force Microscopy

An atomic force microscope (AFM) is a measuring device for different surface properties, as in the simplest case its topography, but many other properties are accessible. The AFM takes multiple data points arranged in a two-dimensional grid with equal distances to visualise the surface properties, these data points are taken one row after the other. Thus, the measuring principle can be related to digital photography based on CCD-cameras, which take optical images with a two-dimensional grid of photosensitive capacitors. In a CCD-camera, the measurement process happens simultaneously: when light falls onto the grid, electrons are excited and stored in each capacitor, each number of electrons representing the amount of incoming light for the different positions. Then, the CCD-grid can be read out row after row by shifting the exited electrons from one capacitor to the next in a controlled manner. The time needed for a read out is usually negligible. This is different for AFM, where the data points are taken one row after the other, which can take up to several minutes.

Atomic force microscopy was invented by Binnig, Quate and Gerber [10]. They implemented it in 1986. Binnig was already involved in the development of scanning tunneling microscopy (STM) in 1982 [11], for which he later was awarded the 1986 nobel prize in physics together with Heinrich Rohrer.

Both STM and AFM use a very sharp tip to interact with a sample surface, achieving the sample topography or other surface properties by scanning over it. For the STM

the interaction between tip and sample is the tunneling current measured during the scan, for AFM the type of interaction depends on the mode used. Many different modes are known for AFM to work properly, each using another type of interaction. The most important modes are the contact mode and the non-contact mode, the former uses a direct mechanical interaction between tip and sample, so that the repulsive Coulomb interaction and Pauli exclusion dominate. The latter non-contact mode drives the cantilever, a small piece of metal holding the tip, to oscillations, increasing the distance between tip and surface. Therefore the attractive van der Waals interactions dominate in non-contact mode.

Both STM and AFM are able to resolve single atoms and chemical bonds, for AFM this has been proven for both main measuring modes (contact and non-contact mode) [12]. The set-up of a typical AFM device is shown in figure 2.1. The tip is mounted on a cantilever attached to a piezo controller. First, we want to limit the discussion to contact mode for the sake of simplicity. When the tip is getting close to the surface and starts interacting with it, the cantilever gets bent. The cantilever is designed such that the force constant allows significant bending when small interatomic forces act on the tip. This bending is measured and thus the tip height can be repositioned to achieve the topography of the sample surface. In the early days of AFM, the bending was measured with a STM tip placed on top of the AFM cantilever. Nowadays, a laser beam is focused onto a small reflecting area on the back of the cantilever to measure the bending. Any deflection or tilt of the cantilever results in a movement of the reflection of the laser beam, which can be registered by a position sensitive device (PSD). The position of the cantilever and thus the tip can be controlled by a piezo element that is able to move in all three directions in space with nanometer precision. The axes parallel to the surface are used to scan the sample, the axis perpendicular is used to control the interaction between tip and sample in the desired way. Typically, the distance is adjusted in order to hold the force acting on the tip constant, but also other modes are possible, for example a feedback with constant current or a constant height scan. Note that in non-contact mode the amplitude or the frequency can be used as a feedback measure, and the deflection signal is used to determine these parameters.

In order to hold a constant force on the tip, the PSD signal is given back into a feedback loop to the piezo element. Thus, if the force becomes higher (or lower) than expected, the piezo controller retracts (or approaches) the cantilever with the tip until the desired setpoint is reached. The reactions of the feedback loop on the differences between setpoint and measured value depends (proportionally) on the momentary difference, the so called error function $e(t)$. In addition, the short time integral over $e(t)$ and its mo-
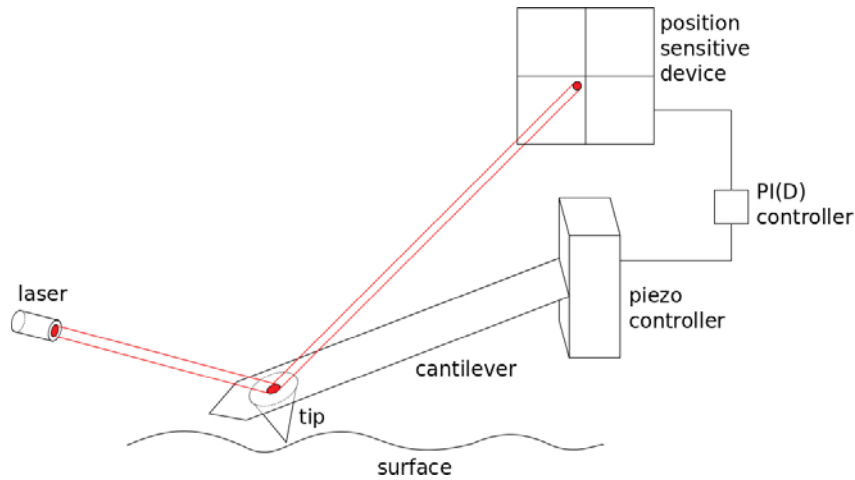
Figure 2.1.: Basic set-up of an atomic force microscope. For working principle see text.

mentary derivative are taken into account. Such a feedback loop is said to be adjusted by a proportional integral derivative controller (PID-controller). PID controllers help minimising the deviations between setpoint and actually measured value. They allow to adjust the gain parameters for each of its components by the experimenter independently. The working principle and the influence of the single parameters is described in detail in subsection 2.1.1.

Unlike STM, which depends on the tunneling current measured between sample and tip as the basic interaction, AFM is not restricted to highly conductive samples, since it is based on the atomic interactions between outermost atoms of the tip and the surface atoms. These interactions are basically described by long range van der Waals forces, Coulomb forces and Pauli repulsion. Other interactions like e.g. capillary forces and magnetic interactions may play a role, and can be used to set-up special measuring modes. In a simplifying model, the sum of the main interactions can be approximated by a Lennard-Jones potential as shown in figure 2.2. Depending on the mode used one can either measure with repulsive or attractive forces between tip and surface. Contact mode is restricted to repulsive forces, while in non-contact mode one can measure both in the repulsive or attractive regimes. When measuring in the repulsive regime in non-contact mode one often calls this tapping or intermittent contact mode.

Since the invention of AFM many improvements and different measurement techniques were developed. In addition to contact mode, where the deflection itself is used to readjust the tip position, one can use non-contact mode, where the cantilever is excited to oscillate, and the oscillation amplitude or frequency are used as a measure for the sample-tip interactions. Attractive long range forces dominate in non-contact mode, thus minimising the interaction forces and the change induced by the tip on the sample. For the measurements
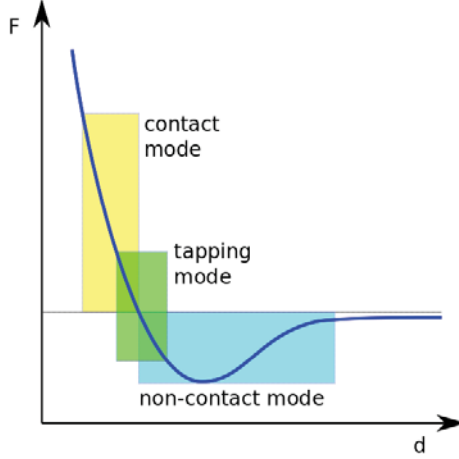
Figure 2.2.: Lennard Jones model for the force distance dependency between tip and sample surface. The regimes in which the different measuring modes work are highlighted. Tapping mode is a subtype of non-contact mode where one can also use repulsive forces.

presented in this thesis we mainly used conductive atomic force microscopy (C-AFM). C-AFM uses a conductive tip (e.g. a PtIr-coating on a Si-tip) to enable measurement of the current flowing between tip and sample when a bias voltage is applied. Thus, C-AFM can visualize the conductivity of different regions on the surface. In addition, C-AFM allows to take I-V-characteristics on any specified spot on the sample surface. With different set-ups, and in some cases special tips, one can also characterise sample elasticity, surface potential (Kelvin probe AFM), magnetic dipole-dipole interactions and many others. In the scope of this thesis various characteristics of an AFM device are important, thus the following sections focus on specific details to facilitate comprehension of this study. The interested reader may refer to the literature for further information [12][13].

2.1.1. PID controller

A PID controller is a device to control the feedback in a feedback loop. PID is an abbreviation for proportional, integral and derivative, corresponding to the way the feedback signal is handled. This can be expressed as

$$f(t) = P_{\text{gain}}e(t) + I_{\text{gain}}\int_0^t e(t)\,\mathrm{d}x + D_{\text{gain}}\frac{\mathrm{d}}{\mathrm{d}t}e(t) \tag{2.1}$$

were $f(t)$ is the output of the PID controller, P_{gain}, I_{gain} and D_{gain} are the constants for proportional, integral and derivative gains, respectively, which are controlled by the user and changed for every specific operation. The error function $e(t)$ is the difference between

current value and setpoint, in the case of AFM the difference between presently acting force and force setpoint. The output of the PID controller $f(t)$ is then given back to the piezo controller in order to move the tip appropriately. In AFM operation one often uses only P_{gain} and I_{gain}, setting $D_{\text{gain}} = 0$. The derivative gain is not necessary to achieve stable images. Nevertheless, adjusting a PI-controller is more of an art then science.

However, with properly set gains, the tip is following the sample surface with a slight delay only. If the gains are chosen too small, the delay may not be negligible anymore, leading to deviations from the true surface and introduce high friction between tip and sample (in contact mode), if the tip is not retracted properly. On the other hand, a too high gain causes the tip to retract too far after an abrupt rise (overshoot). The high gain then leads to a fast approach back to the surface, overshooting again, this time coming too close, which results in (damped) oscillations around the setpoint. In contact mode, if the tip approaches the surface very fast, this leads to high forces acting between tip and sample. The energy lost due to damping is actually transferred to the sample surface. When measuring 3TBT crystals with hundreds of nm up to several μm in height, a too high gain can lead to more or less uncontrolled oscillations. Each time the tip hits the crystal, it transfers energy from its fast movement to the crystal, which can damage the crystalline structure. When far too high gains are used, one can compare the movement of the tip with that of a rapid, scarcely controlled hammer. In subsection 3.2.3 on page 37 we show how this can be used to examine and manipulate the mechanical properties of the crystal structure.

2.1.2. Contact mode

As already mentioned, in contact mode the tip stays in direct contact with the sample and the deflection of the cantilever is used to adjust the tip height. The tip is first approached until the deflection of the cantilever in contact reaches a preset value, the setpoint. Obviously, contact mode works in the regime of repulsive forces (figure 2.2), usually the forces acting in contact mode are much higher than in non-contact mode.

In this study the inclination between tip and surface is of special interest. In figure 2.3 the tip position is sketched in more detail. The scanning direction can be adopted by the user, such that a change in scanning direction changes the direction of the movement of the tip, while the cantilever orientation itself stays the same. Since the cantilever is not aligned parallel to the surface, the tip is inclined on the surface in direction of the cantilever axis. Usually, the scanning direction is along the x-axis as indicated in figure 2.3. Then the tip sample interaction is symmetric for trace and retrace of a scan,

except for the tip point being slightly shifted to the left or to the right of the tips conical body, when viewed in scanning direction. However, it is easily possible to adjust the piezo scanner movement to any linear combination of the scanning axes, resulting in movements in any direction on the plane. We define the scan angle θ as the angle between scanning direction and x-axis. If, for example, the scanning direction is adjusted along the y-axis ($\theta = 90°$), trace and retrace are different, since in one case the tip moves forward with the tip point in advance of the conical body, and in the other case the tip point follows the movement of the conical body. For any scan angle other than 0° or 90° the tip point moves both shifted to the right (or left) and to the front (or back) of the conical body. Note that always both shifting directions occur in each scan, the one in the trace and the other in the retrace scanning.
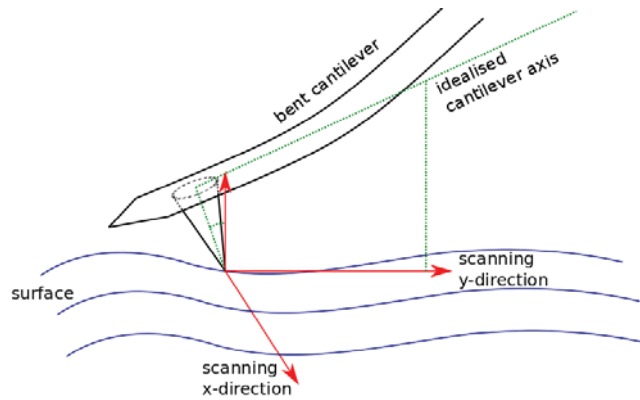

Figure 2.3.: Sketch of a tip in contact with a surface (blue). A coordinate system with the scanning directions as x and y-axis is drawn in red. The coordinate system is defined such, that the projection of the (ideally unbent) cantilever axis is parallel to the y-scanning direction.

The total distance between the center of mass of the tip body and the tip point is influenced by the inclination between cantilever and surface and the bending of the cantilever. The inclination between cantilever and surface is mainly given as a device parameter, with a slight influence given by the surface topography. The bending is influenced by both the cantilever force constant and the force setpoint. The size of the projection along the scanning axis and perpendicular to the scanning axis is then given by the scan angle.

For most samples measured in AFM this is not a relevant property for two reasons. First, for many objects in AFM it is not important if they are aligned with respect to any of the scanning directions or not, secondly, most samples are rather smooth, so that it is not of importance if the tip point follows or advances its body. However, in this work we examine crystals with a height in the µm range, where this can have an influence on the investigated sample. When the tip moves over very steep slopes, as it is the case on

the edge of the crystal, the PID controller may not be able to hold the forces constant, and the tip may not get retracted fast enough. Note that adjusting the PID is always a trade-off between avoiding uncontrolled oscillations and the ability to retract fast enough to avoid high deviations from the setpoint. Thus, when a too low gain is chosen, the tip point might get stuck at the edge of the crystal. This could happen more easily when the tip is advancing its body then when following or moving with a perpendicular shift to the scanning direction. Note also that the long needle-shaped crystals are better suited to be scanned across their cross profile, thus perpendicular to their long axis, since they are much too long to fit into a single AFM image (with reasonable scan time and resolution). Thus the scanning direction really has to be changed for many crystals. Rotating the sample instead of the scanning direction can be a much more complex task, since it at least includes retracting the tip. For some AFM devices it is not accessible after sample preparation anymore. We discuss the consequences of this phenomenon in experiments later (in subsection 3.2.2 on page 35).

2.1.3. Non-contact mode

In non-contact mode AFM two feedback modes have been developed. The amplitude modulation and the frequency modulation mode. Amplitude modulation was developed first and it is easier to implement than frequency modulation. Thus, we want to discuss amplitude modulation mode first, where the cantilever is driven with a constant excitation frequency and a constant excitation amplitude. The excitation frequency is chosen to be close to the resonance frequency of the free cantilever, but usually not set to the exact resonance frequency. If an external force acts on the vibrating cantilever, its resonance frequency changes, i.e. the hole resonance peak is shifted to lower frequencies when an attractive force acts on the tip, and similarly a repulsive force leads to a shift of the resonance peak to higher frequencies. Because the excitation frequency and amplitude stay the same independent of the interaction, the resulting oscillation amplitude changes. Assuming the excitation frequency is set to be slightly lower than the free resonance frequency, an attractive force causes the oscillation amplitude to increase, and a repulsive force causes a decrease of the amplitude, respectively. Since the oscillation amplitude can be measured with the PSD, this mode allows measurements of the surface topography without the high forces induced by the tip sample interaction in contact mode. The phase shift between excitation can be related to the dissipated energy [14]. Thus the amplitude modulation mode allows visualisation of the dissipated energy via the phase image, so that one can distinguish for example crystalline and liquid phases in the nanoscale [15].

However, the experimenter has to be careful when using amplitude modulation. If the resonance peak is shifted towards the excitation frequency, the current resonance frequency might pass the excitation frequency. If this happens, the amplitude first increases and then decreases again (as it changes the edge on the resonance peak). Since the feedback loop can not differentiate the direction of the shift through the measurement of the amplitude, two fundamentally different regimes for measurements exist.

In frequency modulation mode there is no additional regime depending on the preset parameters, since the cantilever is always driven at its resonance frequency. This is done by driving the oscillation with a 90° phase shift. As the driving frequency in such a feedback is always equivalent to the current resonance frequency, the frequency shift can be measured easily and then be used as a direct measure for the tip sample interaction. During scanning, the oscillation amplitude is held constant with an additional feedback loop. This also allows to quantify the dissipated energy in frequency modulation mode, as the driving amplitude then gives a direct measure of the damping.

Amplitude modulation can only be used in air and liquids, but not in vacuum. This is due to the very low damping in vacuum. A high quality factor, equivalent to a low damping, results in a slow relaxation of the amplitude over time. Thus a reasonably fast scan in amplitude modulation mode is only possible in a highly damped system. For frequency modulation, where the cantilever is driven at its resonance frequency externally, there is no need to decrease the scan speed when using a cantilever with high quality factor (low damping). Thus, using frequency modulation is, in contrast to amplitude modulation, well suited for AFM in vacuum.

2.1.4. Conductive AFM

Conductive AFM (C-AFM) allows to measure the current flowing between sample and tip when applying a voltage. In contrast to STM, which can not detect forces and thus needs the current as feedback signal, C-AFM is able to act on insulators as it can use the cantilever deflection signal as a feedback signal and measure the current signal independent of the feedback loop.

C-AFM is driven in contact mode, but one uses conducting tips or tips with conducting coatings. In the scope of this study we used Si tips with PtIr-coating from Nanoscope. As alternatives to PtIr-coated tips among others also Si-tips are used, but those oxidise in air left with an isolating SiO_2 layer and can therefore only be used in UHV. In order to avoid changing parameters without a good reason, the measurements shown here, even those which were taken in contact mode, are taken with the same tips. This holds true

for all used devices. Note that contact mode measurements do not differ from C-AFM measurements with applied bias voltage $U = 0\,\mathrm{V}$, if one uses the coated tips in contact mode.

2.1.5. AFM in Ultra High Vacuum

Running AFM under ambient conditions has several disadvantages. First of all, water can condense on the surface and leave a water meniscus or film. This may lead to artifacts in the images, and besides that may have a big influence on conductivity measurements, e.g. when water has a higher conductivity than the investigated sample. In addition, when cooling the sample below $0\,^\circ\mathrm{C}$ the tip can freeze to the sample, making measurements with low temperatures impossible. Using ultra high vacuum (UHV), at a pressure in the order of $10^{-10}\,\mathrm{mbar}$, circumvents problems like this, allowing reliable conductivity measurements and a widely variable temperature range. In addition, the lateral resolution can be improved to the size of single atoms, this has also been achieved in ambient conditions, albeit with greater effort. Investigating the temperature dependence of conductivity would allow further insight into transport characteristics of 3TBT, thus setting up the C-AFM in UHV was one of the primary goals of this study.

2.1.6. AFM devices used

The experiments done in the scope of this thesis were conducted on three different devices. As the initial aim of the thesis was measuring the conductivity of 3TBT crystals with a C-AFM in UHV, we describe the UHV-AFM used. The C-AFM mode and the low temperature control of this device were set-up for the first time in the scope of this thesis. Due to time restrictions and the fact that the focus changed from charge transport measurements to measurements of the mechanical properties of 3TBT, we needed a device which enables an easier access then the complex UHV system allows. For these measurements we used an AFM in air, also located in Freiburg. Unfortunately, this second device did not allow reliable conductivity measurements in air, thus a third device in air was used, which was provided by a cooperation with nearby university in Mulhouse. In the following we describe these three devices, starting with the less complex devices in air and closing with the UHV system.

JPK (air)

The AFM fabricated by JPK is set up in ambient conditions. It is equipped with two magnifying cameras, one from the bottom and one from the top. The sample is put

horizontally, the tip scanning from the top, mounted on a transparent glass block. The maximum scanning area is (100 µm x 100 µm) The maximum elongation of the piezo-tube used for scanning and approaching the sample surface is 15 µm. With the help of the bottom view camera and an external optical microscope it is easily possible to define the tip position to a specific area on any sample, thus enabling us to relate the crystal measured in AFM with the one seen in optical microscopy (and vice versa), even if crystals are directly next to each other.

Using C-AFM on this device restricts the optical devices to the top view camera only, since the sample bias is applied through an intransparent mounting plate. This makes it harder to identify the position on the sample, while still allowing to approach a crystal with the help of the topview camera. The first C-AFM measurements on this device where taken in the scope of this study. Unfortunately, the current signal showed an irregularly, as far as we can tell purely randomly, appearing and disappearing 50 Hz noise. The origin of the noise could not be detected in the limited time given, the various attempts to screen it with a Faraday cage were not successful. Therefore this device was used mainly to investigate the origin of the breaking of 3TBT crystals.

Bruker (air)

The AFM from Bruker is located at Université Haut Alsace (UHA) in Mulhouse, France. It is equipped with a Multimode AFM head using Nanoscope V electronic [16]. The device is capable of doing both AFM and STM in ambient conditions, scanning from the top with a horizontal sample. The tip is mounted in a transparent plastic holder. The device is equipped with a (gray scale) topview camera with a rather large magnification and good illumination. Thus it is easily possible to choose a crystal and relate the position to microscopy images of the same sample. In contrast to the device manufactured by JPK, where the tip position is related to an external microscope, the microscope is directly included but lacks any additional features like crosspolarisers. The maximum scanning area for the Bruker AFM is (13 µm x 13 µm) with a maximum elongation of 3 µm.

Performing C-AFM on this device is well known and used for several years, which is why we choose this device for most C-AFM measurements.

Omicron (UHV)

The AFM by Omicron is mounted in UHV and capable of using liquid nitrogen cooling down to about 80 K. In the beginning of this study, the AFM was tested and prepared for first measurements with C-AFM and liquid nitrogen cooling was established. In the

same UHV system there is also a STM mounted in a separate chamber, including a low energy electron diffraction (LEED) microscope. The chambers are connected via a transfer chamber, where new samples and tips can be introduced without risk of loosing the vacuum during the process. Another smaller chamber is equipped for liquid vapor deposition, which was needed for the experiments performed at the STM.

In contrast to the AFM devices in air, the sample is mounted upside down with the tip approaching from the bottom. This is important for the crystals studied, since they can break and then fall off the sample. The UHV chamber adds some restrictions, mainly due to reduced accessibility. In addition, the UHV-AFM has some disadvantages. First of all, the maximum measuring height is reduced to 1 µm, which is sometimes problematic for the purpose of this thesis, because some of the crystals are higher than 1 µm and can not be measured with such a device. The maximum scan area is also reduced to about (8 µm x 8 µm). Secondly, the optical system is mounted outside the chamber and thus at a distance of about 30 cm, which limits magnification, illumination and contrast drastically. In addition, the angle between optical axis and surface is about 45°, introducing parallax. In combination with the rather small scanning area this makes approaching a single crystal a task needing several hours. It is virtually impossible to identify a specific crystal on a sample. Small crystals and such at badly illuminated positions are not visible with the optics at all. Thus it is not possible to relate optical microscopy images to AFM images taken with this device. Since the sample has to be glued to a sample holder, which is then held at a fixed position in the UHV-system, one can not rotate the sample against the tip cantilever axis once mounted. This device was set up to work properly and will be of great use for future research on this topic.

2.1.7. Comparing C-AFM to other charge transport measurement techniques

As already indicated in the motivation for this thesis, C-AFM can contribute as a complementing measurement technique. The established techniques, namely transmission line measurements, four-point probing, dark injection measurements and the time of flight method all have different restrictions. In the following, we want to briefly explain these measurement techniques and compare them to C-AFM. Except for the time of flight method all other techniques rely on the fabrication of macroscopic contacts.

Transmission line measurement

The transmission line measurement facilitates the separation of the resistances of the semiconductor R_s and the contacts R_c. Assuming a set-up with two contacts on a semi-conducting single-crystal at a distance d, the total resistance R_total is simply given as the sum

$$R_\mathrm{tot} = R_\mathrm{s}(d) + 2R_\mathrm{c} \tag{2.2}$$

Note that the semiconductor resistance depends on the distance, while the contact resistances of the two contacts are independent of the distance. Extending this by using a set of contacts with a variety of different distances d_i to the first contact, allows the measurement of the semiconductor resistance depending on the distance. As the length dependence is (usually) linear, this allows to extrapolate using linear regression. The value of $2R_\mathrm{c}$ is given as the y-intercept. Thus this method allows to determine the contact resistances. In addition, the semiconductor sheet resistance can be identified via the slope of the linear regression [5].

Four-probe measurements

Four-point probing is a measurement technique for very low resistances. The basic idea is to circumvent the contact resistances by measuring the voltage drop over the resistor without the contact resistances, and the current flowing through it independently, and then calculating the resistance via Ohm's law. This can be realised the following way: Four contacts are attached to the resistor, the bias voltage is applied on the outer two contacts and the current flowing is measured on these. The inner two contacts are used to measure the voltage drop over the device under measure. The big advantage of this set-up is essentially given by the fact that now the contact resistances between voltmeter and the resistor under measure are set in series with the voltmeter and not in series with the resistor. Thus the contact resistances are negligible with respect to the internal resistance of the voltmeter. The technique also allows to determine the contact resistance [6].

Dark injection space charge limited current measurement

In the dark injection method, the organic layer under measure is contacted with an anode and a cathode. The anode contact should be ohmic, the cathode should be an electron blocking Schottky barrier if the hole injection is examined, or the other way round if electron injection is measured. When applying a voltage pulse, the mobility of the semiconductor can be calculated from the characteristics of the measured current.

First, the dark injection current rises until reaching its maximum value, than the current approaches its asymptotic value (the space charge limited current). The characteristic time scale is related to the mobility. The technique is limited due to the fact, that the fabrication of ohmic contacts is error-prone [17].

Still, the quality of the contacts has a significant influence on the apparent mobility and depends on the contact material, purity and time of the exposure of the contacts to air, as for example shown with four-point probing by Zimmerling et al [18]. In addition, the mounting of contacts onto single crystals has been shown to introduce dislocations into organic semiconductor single-crystals [8]. Thus, a method that does not use microscopic contacts can circumvent these unwanted contact effects. C-AFM can be used without applying additional contacts onto organic semiconductor single-crystals. The time of flight method allows this also, but has other limitations. Obviously, when one is interested in the specific properties of applied contacts, as the contacts are needed in nearly every application, the transmission line method for example is still of great use. But, in contrast to the well known and established techniques, which only allow to calculate the mobility of the crystal with applied contacts, C-AFM allows a real measurement of the unaltered semiconductor properties without any macroscopic contacts.

Time of flight measurements

The set-up for using time of flight measurements is somehow similar to the one used in the dark injection method. The organic semiconductor is put in between two electrodes, where a potential is applied. Through one of the (transparent) electrodes a short light pulse is sent to the organic semiconductor. It is absorbed at the surface, producing free charge carriers. These free charges then drift to the other electrode and give a measurable signal from which one can conclude the charge transport properties of the material. The advantage of time of flight measurements over the dark injection method results from avoiding the injection barrier caused by the contacts. In principle, the electrodes are only used to apply the potential, which is needed to cause the drift of the charge carriers, a physical contact to the sample under measure is not necessary [19]. The method has been developed further and can also be used without charge carrier injection with a light pulse, where charge carriers are indeed injected via the electrodes, but the contact resistance can be avoided by applying voltage steps dynamically [20]. However, time of flight measurements are limited to rather thick (several µm) samples in order to achieve an adequate flight distance.

2.2. Crystallisation

In this section we want to compare several different crystal growth techniques, namely physical vapor transport, growth out of solution and out of the melt. Then we briefly discuss birefringence, an optical phenomenon caused by anisotropic crystalline structures.

2.2.1. Growth from physical vapour transport

Growing organic semiconductors through physical vapour transport has been the mostly used preparation technique of organic semiconductor single-crystals for a decade. The principle, proposed by Laudise et al [21], bases on heated gas flowing over the source material in a relatively simple tube arrangement. The tube can be separated in four parts, where the gas is heated in the first part by a resistance wire wound around the tube. In the second part, the hot gas flows over the source material, which then evaporates. Subsequently, the gas cools down and the crystals grow in the next part of the tube. Finally, the remaining material is deposited in the last part.

With this method, many different organic semiconducting single-crystals can be grown, as for example oligothiophenes, pentacene [21] and rubrene [22]. This technique has been studied intensively with respect to the influence of the various control parameters, e.g. temperature and gas flow [23]. The crystal morphology and size can be controlled, and for some molecules sizes up to the cm scale are accessible [24]. Recent progress in the technique also allows to directly grow the crystals in ordered structures [25].

2.2.2. Growth out of solution

To grow crystals from molecules dissolved in a solvent, the solution has to be supersaturated, meaning there are more molecules in solution than allowed by the thermodynamic equilibrium concentration. This can either be done by removing solvent by evaporation and thus increasing the concentration, or by directly changing the thermodynamic equilibrium concentration. The latter can be achieved either by adding another solvent with a lower solubility with respect to the solved molecules or by cooling the solution, using the temperature dependence of saturation concentration, which for most systems decreases with decreasing temperature.

Still, crystallisation may not start in a supersaturated system, if there are no nuclei where the molecules can attach to. If there are foreign particles allowing the molecules to attach to this nucleus, this is called heterogeneous nucleation. For very pure solvents, homogeneous nucleation occurs when reaching a high supersaturation or, for lower con-

centrations, when allowing for long waiting or induction times. A nucleus then forms directly out of solution through accumulation of molecules by chance, but it needs to reach a certain minimal or critical size r_{crit} in order to be stable against dissolution. Since the critical size for a specific molecule can be rather large, this can lead to long-lived meta-stable situations even with a very high supersaturation. A nucleus has reached its critical size when its crystal free energy overcomes the surface free energy needed to form such a nucleus. The critical size depends on the surface energy γ, molar volume ν of the solvent, the temperature T and the supersaturation S as shown in the following equation [26].

$$r_{\text{crit}} = \frac{2\gamma\nu}{k_{\text{B}}T\ln(S(T))} \tag{2.3}$$

Since surface energy and molar volume are constants for a given system, one can increase the probability of spontaneous nucleation (i.e. reducing the critical size of a nucleus) only by increasing temperature or supersaturation. Note that supersaturation itself depends on the temperature, thus cooling actually does not increase the critical size of a nucleus but decreases it.

Once stable nuclei are formed, growth begins. Simplified, the growth process can be dominated either by the surface interaction or by diffusion, whichever process is slowest [26]. If the surface interactions are anisotropic, as it is the case for many organic molecules, the growth rates can have large differences in each direction, thus forming anisotropic crystals. 3TBT, which we describe in more detail later, forms long and slim rods with pointed ends, a shape looking like a needle.

In principle, crystal growth out of solution is easier processable than growth out of the vapor phase, but obviously it can only be processed at all if the molecules are solvable [27]. As for growth out of the vapor phase, crystals various techniques allow deposition of ordered structures on the substrate out of solution [25]. The TBT family studied here is designed to have appropriate side groups to be solvable in common solvents.

2.2.3. Growth out of melt

A third approach to form polymer and oligomer crystals on a surface can be realised through the melt or thin film. For this purpose, molecules are solved and the solution is spin coated onto a substrate, thus forming an amorphous thin film. In this procedure the film thickness depends on the spin speed and the concentration of the molecules in the solution. Annealing the film increases the mobility of the molecules, thus allowing them to reorient and eventually form stable nuclei and subsequently small crystals when hold at a constant temperature. The morphology of the crystals depends on various parameters,

such as film thickness, crystal growth rate and temperature and the interactions between sample and molecules. Many different morphologies and sizes can be grown in a controlled manner out of a thin film by varying the growth conditions as the crystallisation temperature and film thickness, for example hexagonal and dendrite structures [28] and stacked crystalline lamellae with the same orientation in multiple stacks [29]. The TBT family was shown to form both needle-like and plate-like structures when grown out of melt.

2.2.4. Birefringence

If an optical medium has an anisotropic refractive index, it is called birefringent. This effect is well known since 1669, when it was first described in calcite crystals, that split an incoming (and unpolarised) beam into two separate beams. One of these beams follows snell's law, while the other one violates it. The polarisations of these two out coming rays stand perpendicular to each other. The effect can be explained by either a non-cubic crystal symmetry or the order of the dipole moment of the molecules in a crystal. As Richard Feynman stated in his famous lectures: "[But] long needlelike crystals undoubtedly contain molecules that are asymmetric, and one observes this effect very easily" [30]. In addition, birefringence can be induced by stress, one of the major applications in industry, since the polarisation state of transmitted light allows the identification of components under stress.

In the simplest case, a crystal has two different refractive indices, the ordinary refractive index n_o along the so called optical axis, and the extraordinary n_e in every direction perpendicular to it. As a measure for birefringence, the difference $\Delta n = n_e - n_o$ is used. In principle, one can distinguish positive and negative birefringent materials, depending on the sign of Δn. In other words, if the extraordinary refractive index is larger than the ordinary refractive index, a material is called positively birefringent, else negatively birefringent. In the more general case of three different refractive indices, one calls the material biaxial, since there is no single optical axis anymore. Obviously, in this case it is not possible to define an easy measure for the birefringence. This general concept is much more complex, thus we limit ourselves here to the discussion of uniaxial birefringent media.

Depending on the incidence angle between ray of light and optical axis, the beam may be split into two orthogonally polarised beams (if it was unpolarised in the beginning). This is the case if the incident ray is neither parallel nor orthogonal to the optical axis, two special cases we want to discuss separately. The Huygens-Fresnel principle helps

describing the effects of birefringent media. While in optically isotropic media elementary waves are spherical, they become ellipsoids when the refractive indices are anisotropic. In uniaxial media, these ellipsoids are rotationally symmetric around the optical axis (note that this is not true for biaxial systems). In the first case (parallel), there is no difference for differently polarised light as in uniaxial media the refractive index is the same for any orientation perpendicular to it, thus having no influence on different polarisations. In the second case (orthogonal), the beams do not split into separate beams, but differently polarised light has different phase velocities, thus changing the phase between ordinary and extraordinary polarised components. In terms of the Huygens-Fresnel principle, the elementary waves are stretched in negative birefringent media or compressed in positive ones. This can be used as a so called waveplate, to e.g. turn the polarisation direction of a linearly polarised incident beam depending on the thickness of the plate.

If the incident beam has any other direction, the propagation direction of the extraordinary beam (with polarisation parallel to the optical axis) depends on the angle between optical axis and incidence, as the optical axis defines the orientation of the ellipsoidal elementary waves, and thus the resulting wave front.

In this study we use the birefringence as a method to identify the orientation of the molecules in the single crystal, since the molecules have a high transition dipole moment along their backbone.

2.3. Studies on the TBT family

This thesis contributes to the research on conjugated polymers, focussed on the TBT family of molecules. The name TBT abbreviates the structure of the monomeric unit, consisting of two thiophene rings (denoted by T) enclosing a benzene ring (denoted by B). The TBT family is subdivided into two subgroups, which differ in the sidechains attached to the benzene ring. This can be either an octoxy group, which results in calling the TBT unbranched, or an octoxy group with an ethyl group attached at the first carbon of the chain, referred to as branched. Both branched and unbranched molecules where synthesised with lengths ranging from 1TBT to 7TBT. In this thesis we investigate mainly unbranched 3TBT, but also have a look into branched 5TBT. Figure 2.4 shows the chemical structure of those two molecules, both as representatives for the branched and unbranched groups, and also as the two molecules which were examined in the scope of this thesis.

The TBT structure is designed especially as a model system for conjugated oligomer semiconducting single crystals. The backbone consists of thiophene and benzene, both
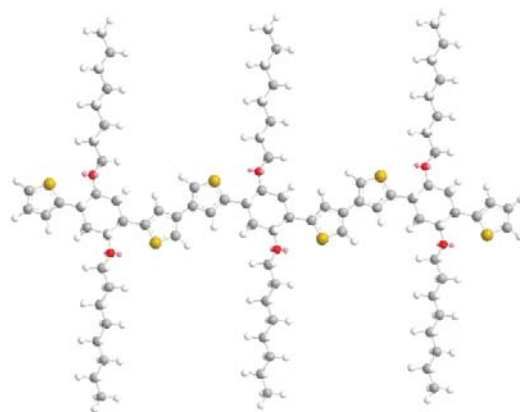
(a) Unbranched 3TBT.
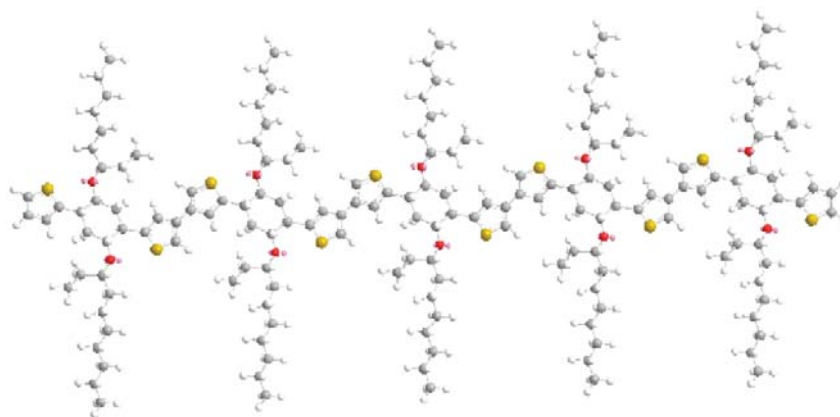
(b) Branched 5TBT.

Figure 2.4.: Chemical structure of the molecules used in the scope of this thesis as models for both branched and unbranched molecules in the TBT family. The elements are marked with different colours: carbon grey, hydrogen white, sulfur yellow and oxygen red.

known for their high conjugation, and their supramolecular interaction through π-stacking, which enhances crystal growth. The interaction between the sulfur atoms in the thiophene rings and the oxygen atoms in close vicinity is known to be strong, thus stabilising the backbone in addition. Recently, these interactions were shown to stabilise the backbone of $1,4-$dimethoxy$-2,5-$bis$(2-$thienyl)benzene [31], a very similar structure to 1TBT (1TBT with methoxy groups instead of full sidechains). The structure shown in figure 2.4 takes this interaction into account, thus the thiophene rings are drawn aligned, such that the sulfur atoms in the rings are turned towards their corresponding oxygen atoms. In principle the thiophene rings are able to rotate around the benzene ring bond, but the shown conformation is energetically more favourable because of the sulfur-oxygen interaction.

Its sidechains enhance solubility in organic solvents to simplify processability. Higher molecular weight increases the conjugation length along the backbone of the molecule. But since increasing the length of the backbone is decreasing solubility, the branching in the sidechains was introduced in order to regain solubility. On the other hand, branched sidechains hinder the crystallisation process, thus both branched and unbranched structures were designed to compare the different molecular structures. Short members (with up to 3 or 4 monomer units) of the TBT family are expected to be soluble in their unbranched structure, while longer TBT members can be dissolved only in the branched configuration. The resulting differences in solubility, crystallisation, optical and charge transport properties are interesting future topics for themselves. This may lead to new insight in molecular design.

Monolayers of a mixture of 2TBT and 3TBT on graphene were studied by Shokri et al [32]. They used a mixture of 2TBT and 3TBT deposited onto graphene, 2TBT and 3TBT phase separated into distinct regions, which mainly consisted out of one or the other oligomer length. The molecules self assembled into monolayers consisting of TBT wires separated and electrically isolated by their octoxy side chains. They found that the end thiophene rings in TBT physically linked neighbouring molecules via π-stacking, and observed a continuous density of states reaching over several molecules. This continuity possibly leads to supramolecular charge delocalization and thus excitonic energy transport over large scales. This study gives a promising sign for interesting electrical and optical behaviour of single crystals consisting of TBT family members. It also showed a conformation of the molecules in the monolayer according to the stabilising influence of the sulfur-oxygen interaction on the backbone as discussed above.

Unbranched 3TBT, as shown in figure 2.4a, was grown to needle shaped crystals by PhD-candidate Sajedeh Motamen (unpublished work). Dodecane was used as a solvent with the concentrations $c = 0.1\,\mathrm{mg/ml}$ and $c = 0.01\,\mathrm{mg/ml}$. 3TBT was dissolved completely when heating the solution to $100\,^{\circ}\mathrm{C}$. After $3\,\mathrm{min}$ the solution was cooled to $60\,^{\circ}\mathrm{C}$ to start crystallisation by nucleation and growth. After one week large, needle shaped crystals with thicknesses from about $2\,\mu\mathrm{m}$ to $5\,\mu\mathrm{m}$ are grown in a solution of a concentration of $c = 0.1\,\mathrm{mg/ml}$. Those crystals reached lengths up to $800\,\mu\mathrm{m}$. The comparatively fast growth along the needle axis is attributed to π-stacking. Using a concentration of $c = 0.01\,\mathrm{mg/ml}$ leads to much thinner crystals ranging from about $100\,\mathrm{nm}$ to $1500\,\mathrm{nm}$ in thickness. They were still up to several $100\,\mu\mathrm{m}$ long. The crystals width is usually much larger then its height, the differences are in the range of a factor of about 2 to 5. This ratio is, as expected, independent of the used concentration.

As many other organic semiconductors, 3TBT has interesting optical properties. While this thesis aimed at charge transport properties and mechanical properties of single-crystals, Sajedeh Motamen investigates the optical properties of 3TBT crystals. Comparing absorbance spectra of 3TBT in solution and crystalline 3TBT a high red shift can be identified. This is a sign of increasing conjugation and thus of high order.

Investigating the crystals with optical microscopy using crossed polarisers revealed their birefringent behaviour and enabled the identification of the molecular orientation in the crystals. This is a well known technique often used for other organic semiconducting single-crystals, as for example oligothiophene single-crystals [33]. Rotating the crystal long axis with respect to the crossed polarisers, the intensity shows intensity minima and maxima every 45° (see figure 2.5a). Assuming that the transition dipole moment lies along the backbone axis of the molecules, one can conclude that the 3TBT backbones are oriented perpendicular to both the long axis of the crystal and the substrate (compare figure 2.5b). The high dichroic ratio, which is defined as $r = \frac{I_\perp - I_\parallel}{I_\perp + I_\parallel}$, again indicates a high degree of order in the crystals.

(a) Intensity as a function of the angle between polariser and long axis of the crystal, plotted radially with higher intensities having larger distances to the origin. Adopted with permission from Sajedeh Motamen.

(b) Orientation of the molecules in the crystal.
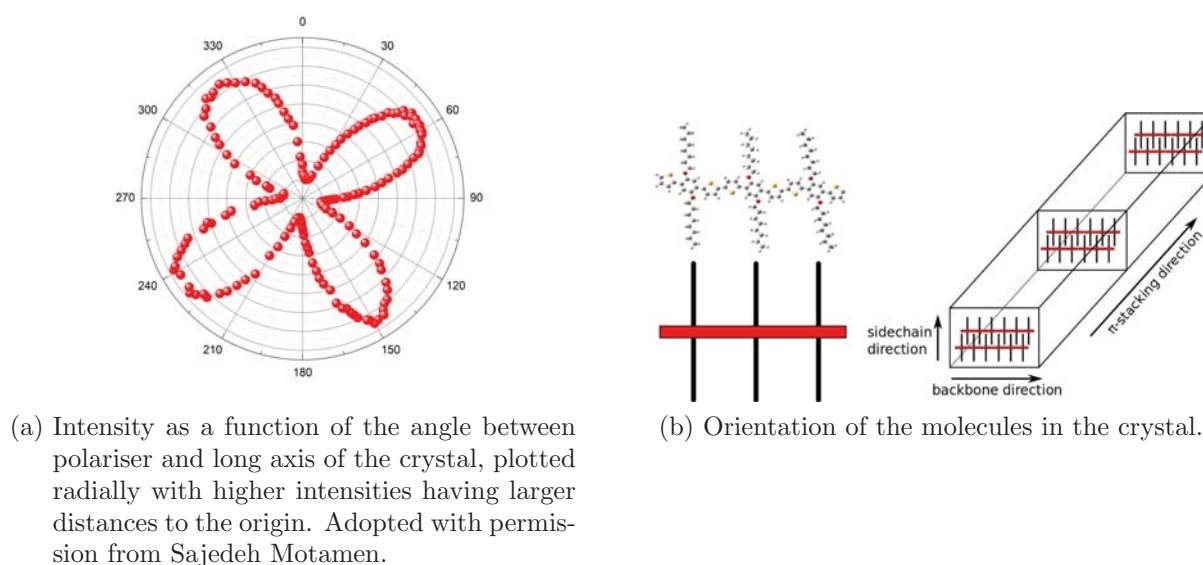
Figure 2.5.

In addition to growth out of solution, crystals were grown out of melt. To achieve this, unbranched 3TBT was solved in toluene at room temperature with a concentration of $c = 1.4\,\mathrm{mg/ml}$. Spin casting $3\,\mathrm{\mu l}$ of this solution on a graphite sample results in a amorphous thin film of 3TBT molecules. Heating of the sample was performed on a Linkam temperature controlling stage for optical microscopy. Heating the sample increases the mobility of the molecules, leading to the formation of many small nuclei at a temperature of 120 °C. Since smaller nuclei are thermodynamically less stable than bigger ones, the

small crystals melt completely when heated further, while the bigger nuclei stay stable. The size of the TBT crystals can be controlled via the growth temperature, since the total amount of molecules stays the same, but the number of stable molecules decreases with increasing temperature, the crystals grow bigger with higher crystallisation temperature. The temperature was held at 150 °C to melt most of the small crystals completely, then reduced to 145 °C and held there to grow the remaining crystals. The crystals shape is similar to the needles grown in solution.

In a similar procedure branched 5TBT crystals were grown. Here a concentration of $c = 2.8$ mg/ml was used. There, the growth of small crystals started at a temperature of about 135 °C. The thermodynamically most stable crystals persisted a temperature of 180 °C, and were grown at 175 °C. Branched 5TBT showed a rectangular plate-like crystalline shape when grown with these parameters. Preliminary results show, that the film thickness plays a major role for the morphology and possibly the orientation of the molecules. In thick films, the crystals form plate-like structures, in thin films, the molecules crystallise in needle-like shapes. It is supposed that in plate-like molecules the orientation changed, a possible explanation would be that the π-stacking direction is perpendicular to the surface, thus the rectangular shape may represent the different growth speeds of the backbone and the sidechain directions.

2.4. Review of related research

Hourani et al studied an oligomer containing 8 monomer units of 3-hexly-thiophene [9]. These molecules have similarities with 3TBT since they as well contain a backbone with thiophene rings and alkyl-sidechains. The molecules denoted with $(3\,HT)_8$ were grown by nucleation and growth in tetrahydrofuran, forming needle-shaped single-crystals. When depositing them onto a substrate, the conjugated backbone of $(3\,HT)_8$ is oriented perpendicular to the surface, and the alkyl-sidechains are lying parallel. This is in contrast to the 3TBT crystals, where the backbone is oriented parallel, and the octoxy-sidechains are perpendicular to the surface. In both cases the long axis of the needle shaped crystal correspond to the π-stacking direction.

In their experiments, they show that the charge transport is anisotropic, with orders of magnitude higher conductivity along the molecular backbone than along the π-stacking direction. This can be shown by depositing a needle shaped crystal partly onto an evaporated gold electrode, and partly onto the underlying insulating Si-oxide, as sketched in figure 2.6. On parts where a $(3\,HT)_8$-crystal is fully placed on such a gold electrode, measurements through the vertical direction, thus along the molecular backbone, are ac-

cessible to C-AFM. The charge transport along the backbone is dominated by Fowler Nordheim tunneling. It is limited by direct tunneling for voltages below a threshold value, which can be interpreted as the tunneling barrier for hopping between two adjacent molecules. If this assumption is correct, C-AFM allows a quantitative measure of crystalline order along the backbone. Depositing the crystal onto an edge between a gold electrode and the insulating SiO_2-substrate allowed current measurements along the long axis of the needle (π-stacking direction) as shown in red in figure 2.6. Space charge limited current dominated along this axis, demonstrating anisotropic charge transport with largely differing mobilities. The mobility value along the thiophene backbone is about 500 times higher than along the π-stacking direction.
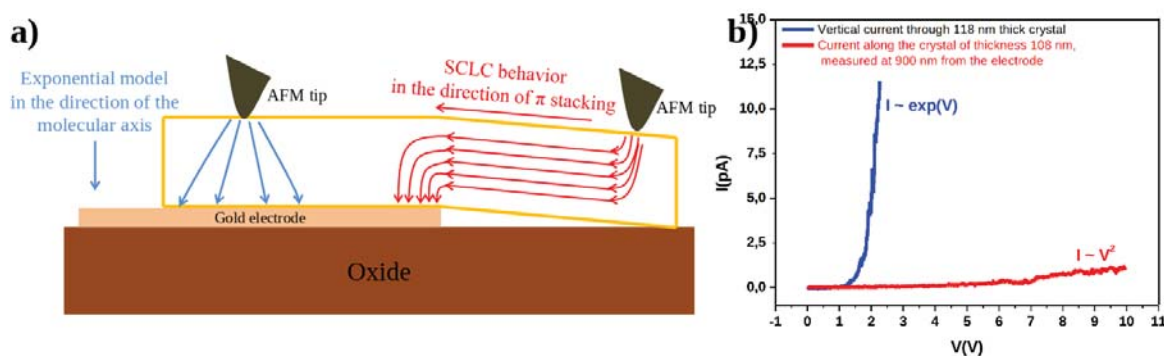
Figure 2.6.: (a) Schematic representation of a single crystal laid on the gold electrode and extended on the oxide showing the vertical current in the direction of the molecular axis as well as the current along the crystal in the direction of the π-π stacking, and (b) I-V characteristics in the vertical direction of a crystal of thickness 118 nm (blue curve) and along the crystal of thickness 108 nm measured at 900 nm from the electrode (red curve). Figure and caption adopted from [9].

Since the resistivity of the crystals depends on volume effects, it is expected to decrease with an increasing crystal cross section, Hourani et al excluded a major contribution of surface effects. Thus they concluded that charge carrier mobility measurements with C-AFM on organic semiconductor single crystals are reliable in air, even though a water meniscus may be present.

2.5. Sample preparation

In the scope of this thesis many different samples were prepared and studied. Sample preparation was done in close cooperation with Sajedeh Motamen, the crystallisation process was conducted solely by her.

We can omit the deposition of the crystals grown out of melt here, since the crystals directly grow on the surface in this case. As a starting point, we deposited crystals out of solution on graphite in order to investigate the charge transport properties on a conducting sample. First, we take a small part (typically a few ml) of the solution with the ready grown crystals and centrifuge the assay for 8 min to 10 min at 8000 rpm. During that time, the suspended crystals accumulate at the lower end of the vial, where one could see them with bare eye. Afterwards we pick the visible spot with a pipette and deposit the crystals on the graphite. Most of the dodecane is removed by spincoating for 1 min at speeds up to 2000 rpm, any additional solvent rest can be removed by putting the sample in a vacuum oven at about 50 mbar over night. This procedure is independent of the used concentration, i.e. crystal size.

As we needed also substrates with higher conductivity than graphite exhibits (see section 3.1), we prepared samples on graphene and SiO_2 samples with gold contacts with the same procedure. The gold contacts on SiO_2 are arranged in a comb structure, where two separated combs are overlapping with alternating teeth with a distance in the μm range. These gold combs can be contacted with silver glue independently.

Samples on glass and SiO_2 substrates were prepared in a similar fashion for the investigation of the optical properties (not shown here).

3. Experiments on mechanical properties of 3TBT crystals

In this chapter we present the measurements conducted with AFM. First, we discuss a misinterpretation of objects observed on graphite briefly. As we began investigation of crystals deposited on graphite, we also examined bulge lines as an inherent part of graphite, misinterpreting them for crystalline structures, due to the fact that we were expecting to see crystals. This can be seen as an example for a biased point of view problem, which is typical for scientific research. We give an explanation on how this mistake developed in order to prevent other similar failure and hope to show ways of realising such a development early on.

In the following section we will describe the experiments investigating the mechanical properties of 3TBT crystals in detail. We show how crystals can be manipulated both in contact and non-contact mode, and discuss other possible influences like tip inclination or applied sample bias.

Finally, the charge transport properties of 3TBT crystals are described, as we investigated them with C-AFM.

3.1. Bulge lines on graphite

3TBT crystals were deposited on graphite as described in section 2.5. Then C-AFM measurements were performed with the Bruker AFM. The crystals were chosen with the help of the integrated optical microscope. It is not possible to distinguish crystals and bulge lines on graphite in a microscope without a crosspolariser. Because the integrated microscope is not equipped with a crosspolariser, we expected both objects to be crystalline 3TBT. With polarising microscopy the difference between crystals and bulge lines is easily visible as one can see in figure 3.1.

Obviously, the crystals and the bulge lines showed extremely different properties in C-AFM. While the real crystals were conducting only very poorly, the graphite bulges did not show any difference in conductivity compared to the surrounding area. In ad-
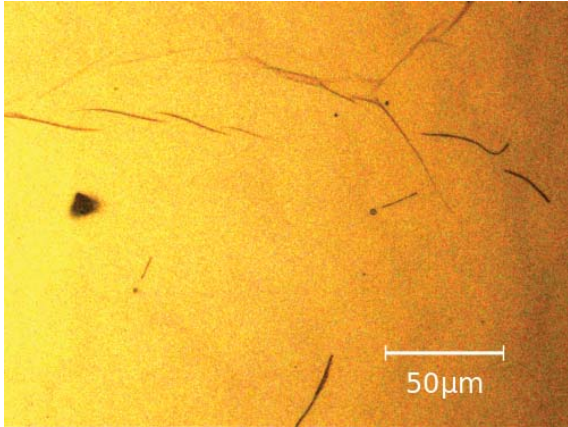
(a) Image taken with optical mircroscope of 3TBT crystals deposited on HOPG. Some of the long needle shaped objects are bulge lines. Distinguishing those from crystals is not possible without a polarising microscope. The Bruker AFM, which is equipped with a mircoscope and a camera provides very similar images.
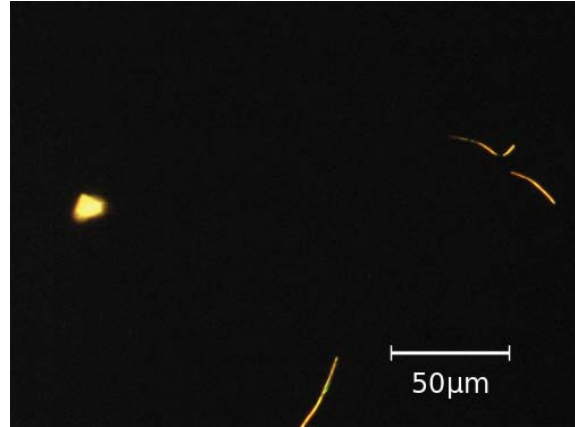
(b) Using crosspolarisers the bulge lines vanish, since they are not birefringent, while the crystals are still clearly visible.

Figure 3.1.

dition, the height profiles were triangular for bulge lines and (nearly) rectangular for crystals. Note that both width and height are accidentally in the same range. We at first supposed two different molecular orientations in the crystals and concluded that the conductivity along the triangular vertical axis (misinterpreted as the backbone axis) is so large, that graphites conductivity is the limiting factor. This theory was at first sight supported by our expectation of large anisotropy in the crystal, namely the expectation of high conductivity along the 3TBT backbone axis. In order to overcome the hypothetical limitation of the substrate, we prepared other samples using substrates with higher conductivity (namely graphene and gold). Since reproduction of these results failed on these substrates, simply because no triangular objects were found anymore, we tried to distinguish between rectangular and triangular objects with optical microscopy. This eventually delivered insight into the true nature of these triangular objects. A time saving methodological approach would have been to check the bulge lines in polarising microscopy before preparation of other samples and subsequent C-AFM measurements. In general, a further testing with any secondary measurement technique can help avoiding mistakes like this. A plain and complete documentation allowing true reproduction of every single measurement should include a distinct identification of crystals, which was in principle available through optical microscopy. This could avoid such a misinterpretation

effectively. For additional information about this topic see section A.1 on page 56 in the appendix.

3.2. Mechanical properties of crystals and breaking

When measuring in contact mode at C-AFM, we observed that some of the crystals break during the scanning. This effect was visible both for UHV measurements and for measurements taken under ambient conditions. Thus we conclude that the breaking is not due to solvent effects of either a water meniscus or rests of dodecane which may not be well evaporated. Measurements on 3TBT needles grown out of melt which broke in a similar fashion reassured this theory. Figure 3.2 shows one of the AFM images taken while breaking a crystal with the AFM tip. Note that it did not break 5 times, as one may conclude from the image, but only on two positions. The changes in position during the scan are due to movements of the crystal piece cut out. These movements were caused by the tip, indicating a very low interaction between crystal and surface. In the UHV system parts that were broken at two positions often fall off the sample, since in UHV the sample is held overhead and scanned from below (see subsection 2.1.6 on page 16). Thus the experiments investigating the breaking mechanism were performed under ambient conditions.
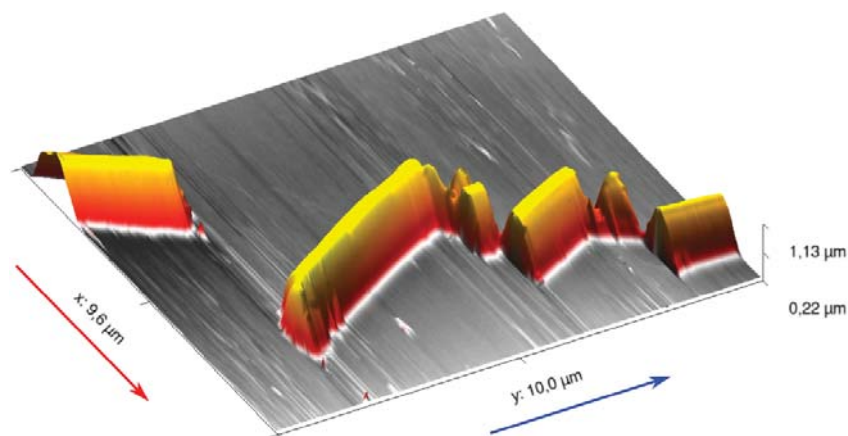
Figure 3.2.: This image was taken on a Au electrode on top of a SiO_2 surface under ambient conditions in C-AFM mode. During measurement the crystal broke and was moved over the surface by interactions with the tip. The fast scanning direction is indicated with a red arrow, the slow scanning direction with a blue arrow, respectively. The image was taken in a mode, where both trace and retrace where measured. The retrace is not shown here, since there were no significant differences.

3.2.1. Investigation of the influence of scanning parameters

The first assumption about the breaking of crystals was a bad choice of the parameter set. The different parameters were checked intensively, in a first attempt we simply applied unreasonably high or low values for different parameters. If any crystal could be damaged by such a parameter choice, this would give good evidence for this specific parameter playing a major role in the mechanics of breaking. For these experiments we approached crystals that were not breaking or unstable from the beginning of the scan. We discuss experiments in unstable conditions in this section also, but begin with the parameter choice.

First, the setpoint was increased up to the detection limit of the PSD, but without any resulting instabilities in the tip movement or changes in the crystal structure. In particular, breaking of a crystal could not be induced with a simple increase in applied force, not even with very high forces.

As a too low gain can cause high friction, especially when measuring high objects as the 3TBT crystals are, we set a very low gain on purpose on a stable crystal. This leads to a much too slow retraction of the tip when coming into contact with the crystal, thus resulting in a high pressure on the sides and edges of the crystal. Again, the crystals were mechanically stable and it was not possible to damage a crystal with such a treatment. Increasing the scanspeed to increase the pressure even further (actually the ratio between scan speed and gains defines the relative speed of retraction), did not change this, either. With such a parameter set imaging was not possible anymore. The tip clearly did not follow the crystal shape anymore. Trace and retrace varied to a high degree, and with very low gains the tip could not reach back to the surface after being pushed away by the crystal. Even when acting with low gains and high setpoints at the same time, none of the examined crystals was damaged. Eventually we can conclude that it is not possible to damage a crystal simply by applying an unreasonable choice of scan parameters.

We also investigated the probable influence of applying a bias voltage to the sample, assuming that a charged tip may snap into contact with the crystal, thus acting with a high force. In principle, such a process should be visible in the vertical deflection image, which consists of the signal caused by cantilever torsion perpendicular to the scanning direction. Such an effect was not observed. Besides this, we observed both breaking of crystals when measuring with very high applied voltages (up to $8\,\mathrm{V}$), as well as when acting without any applied voltage. No significant influence of the bias voltage was seen. Both applying $0\,\mathrm{V}$ and contact mode without connection to the current measuring device were checked independently. Note that we also used conductive tips in (non-conductive) contact mode to avoid any independent but unnoticed parameter change.

Interestingly, some crystals were unstable when measuring. Such an image is shown in figure 3.3. On such a crystal it was not possible to achieve a parameter set for a stable measurement. Instabilities like this are a sign of high probability that a crystal is going to break. This depended sometimes, but not always, on the position where the measurement was conducted on the crystal. The I_{gain} and P_{gain} where set to 90 Hz and 0.002, the scan speed was set to 2.5 µm/s, the setpoint was chosen at 0.5 V. With such a parameter set the measurement was stable and clear on other crystals with the same height. Deviating from this parameter set did not improve the stability of the measurement.
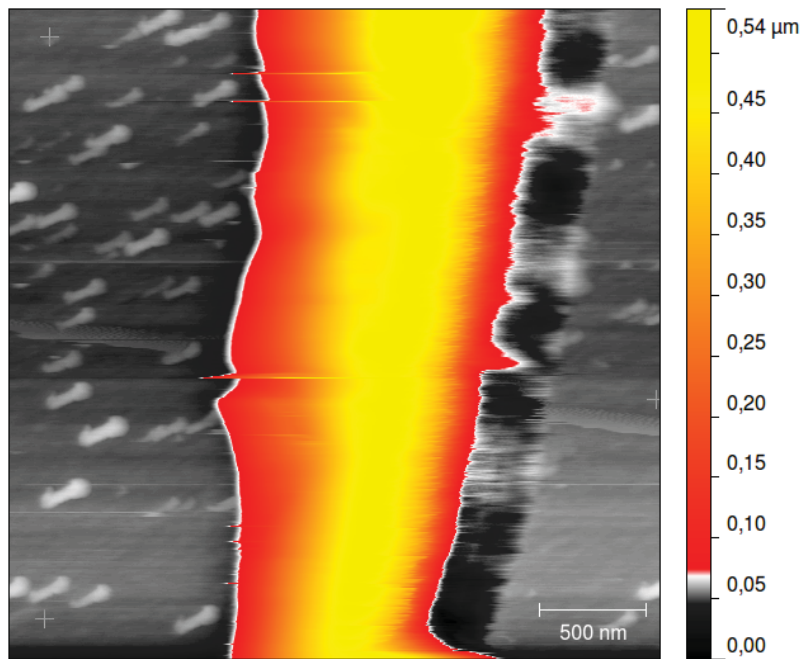
Figure 3.3.: Unstable AFM image.

3.2.2. Chopping with inclined tip

As indicated in subsection 2.1.2 on page 12 the tip is inclined against the surface. Since the crystals examined in this study broke during measurement without obvious reasons, we investigated the influence of scanning direction with respect to this inclination. Theoretically, the tip may get stuck into the crystal if it approaches too fast and with a too high force. In this case it may be possible to cleave the crystal like an axe or pick would. Fortunately this is only true if the scanning direction is not perpendicular to the cantilever long axis as shown in figure 3.4. Clearly, such experiments can only be done

if the sample can be turned easily. The Omicron UHV AFM was not suited for these experiments.
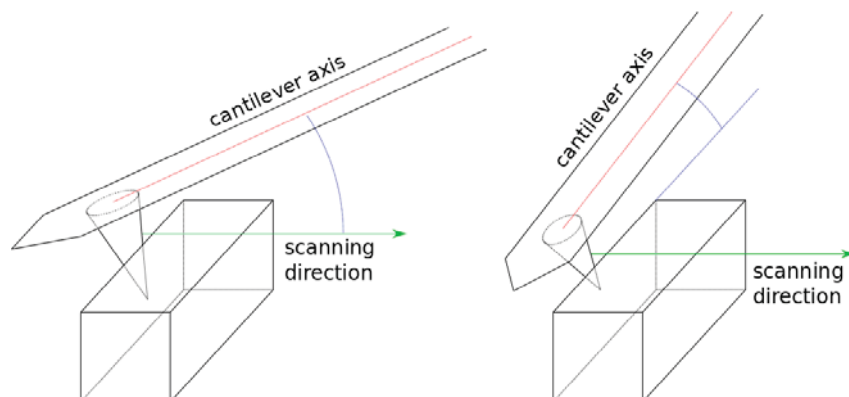
Figure 3.4.: Sketch of the different scanning directions. On the left side the tip moves along the projection of the cantilever axis on the surfaces. Here, the tip can get stuck in the crystal when approaching in scanning direction, since the cantilever is inclined to the surface. On the right side the scanning direction is perpendicular to the projection of the cantilever long axis on the surface, therefore avoiding to chop the crystal.

To quantify if the inclination of the tip against the crystal plays a major role in crystal breaking, measurements are performed with $\theta = 0°$ first, to see whether the chosen crystal is weak and breaks directly or not. If not, the sample is turned by 90 degree and a second measurement is performed on the same crystal. In figure 3.5 polarising microscopy images before and after such a measurement are shown. The crystal shown did not break during measurements performed at several different positions on the crystal, when using $\theta = 0°$. On the first attempt to approach the sample with $\theta = 90°$, the crystal broke and was bent as shown in figure 3.5b.

Clearly, this experimental approach is biased, since it is not possible to scan the crystal over its total length in a reasonable time, one can never exclude that the second approach with inclined tip hit a weak spot in the crystal by accident. It is also not possible to approach the exact same position after turning the sample, since the position calibration is only capable of a precision in the order of $10\,\mu m$ to $20\,\mu m$.

However, such a breaking was observed for 2 other crystals directly after turning the sample to $\theta = 90°$. Contradictory, we as well observe crystals breaking when scanned without inclination between tip and crystal, but it seems to happen more often when measuring with inclination. Still, this is subjectively biased view on basis of a small control sample. To achieve statistical significance to support this theory, many additional of these highly time consuming experiments would be necessary.
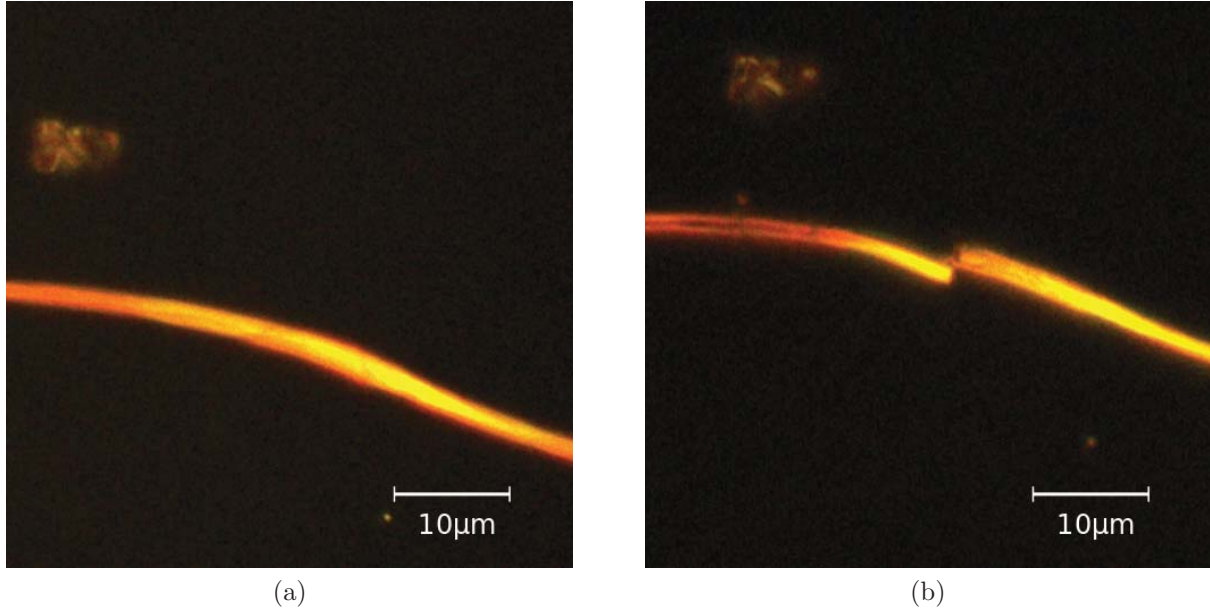
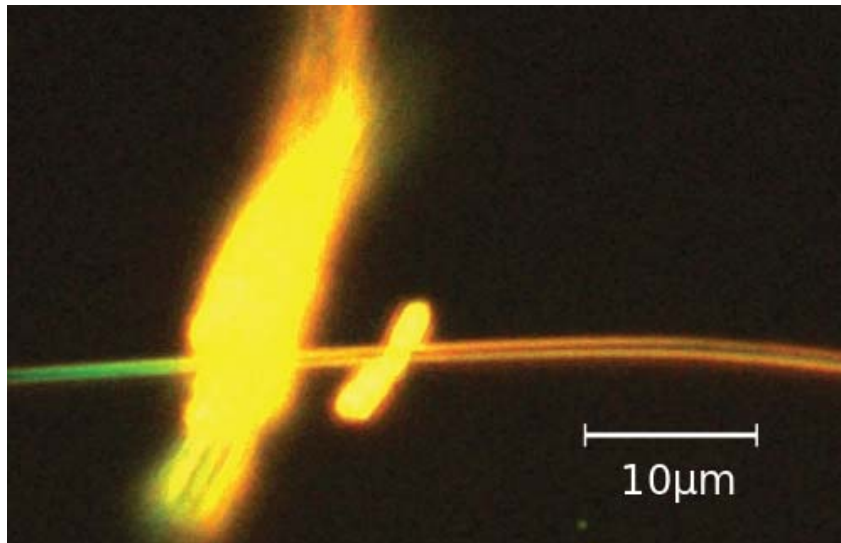Figure 3.5.: Polarising microscopy images before a) and after b) scanning.

3.2.3. Cutting in contact mode

Since normal parameter checks and investigation of chopping with an inclined tip did not yield clear results, we tried to follow another approach. Another possibility to act with high forces on the crystal, is to produce an overshoot on purpose. In the following we describe how we can cut the crystals by hammering with the tip from above. In the next section we deploy this technique also in non-contact mode, where the mechanism is better controllable and yields more insight.

Figure 3.6a shows a crystal grown in solution and deposited on a Au layer on top of SiO_2. In the top part of the image one can see a birefringent object lying on top of the crystal. We suppose it is (at least semi-)crystalline 3TBT. During the scan this object was broken and moved over the sample (compare figure 3.6b). It was not possible to scan the object properly before it was broken and moved, which happened at the first attempt to scan it.

The crystal itself was stable and we could document the initial shape and structure with AFM in contact mode (figure 3.7 on page 40). The image was taken with $I_{gain} = 200\,Hz$, $P_{gain} = 0.002$, $V_{setpoint} = 0.5\,V$ and a line rate of $1.2\,Hz$, corresponding to a scan speed of $5.4\,\mu m/s$. Afterwards the tip was moved to a small area (a small set of scan lines) in the middle of the scanned part. In normal scan mode we scanned a few lines while constantly increasing the P_{gain} until the tip started overshooting. Overshooting began at $P_{gain} = 0.014$. It was intended to cleave the crystal by hitting it with the tip as it

quickly returns following the overshoot. Repeating this process several times at the same position cut the crystal in two distinct pieces, which could be directly monitored with AFM as shown in figure 3.8a. Actually it removed the material layer by layer rather than cleaving the crystal with a sharp edge. Cutting by overshooting was also possible at another position of the same crystal with similar results (compare figure 3.8b). In both images one can see that the underlying Au layer was scratched during this process. Different growth conditions for the crystal as concentration in solution or growth out of melt did not show any influence on the stability against this cutting method. As well, this effect is independent of the used substrates. Unlike the Au layer, other substrates where not damaged with this method.

(a)
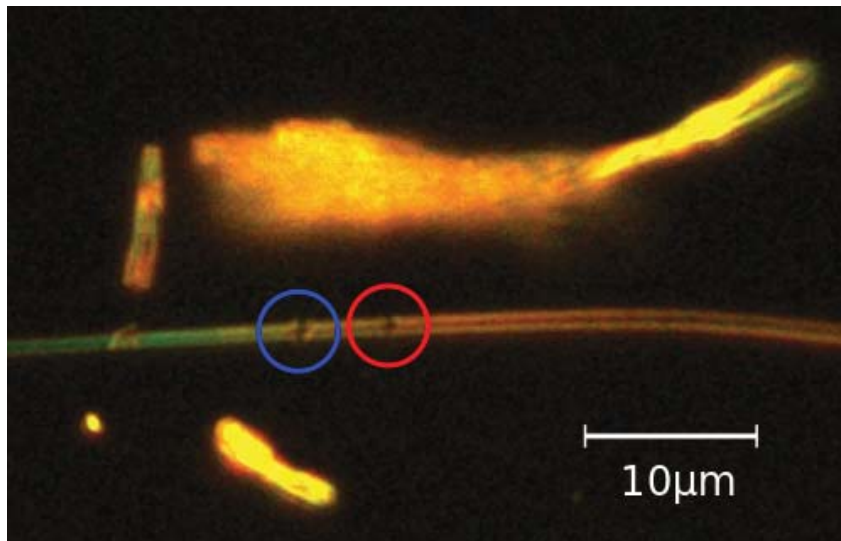
(b)

Figure 3.6.: Images of the crystal taken with polarising microscope. Picture a) was taken before and b) after measuring with contact mode AFM. We cut the crystal at the two positions, marked with red and blue circles, with contact mode AFM by overshooting. The corresponding AFM images are shown in figures 3.7, 3.8a (both blue) and 3.8b (red).
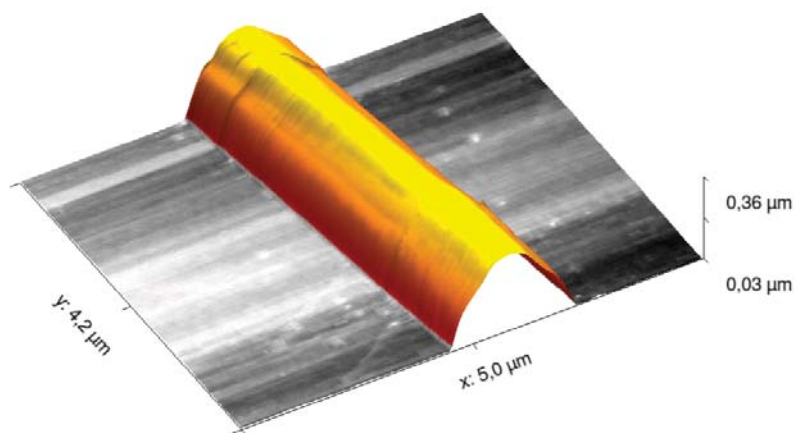
Figure 3.7.: AFM image taken in contact mode, this crystal was grown in solution and deposited on the SiO_2 sample with Au electrodes. The crystal lies fully on one of the Au electrodes. After taking this image we set the tip to its center and cut it by overshooting.

(a)

(b)
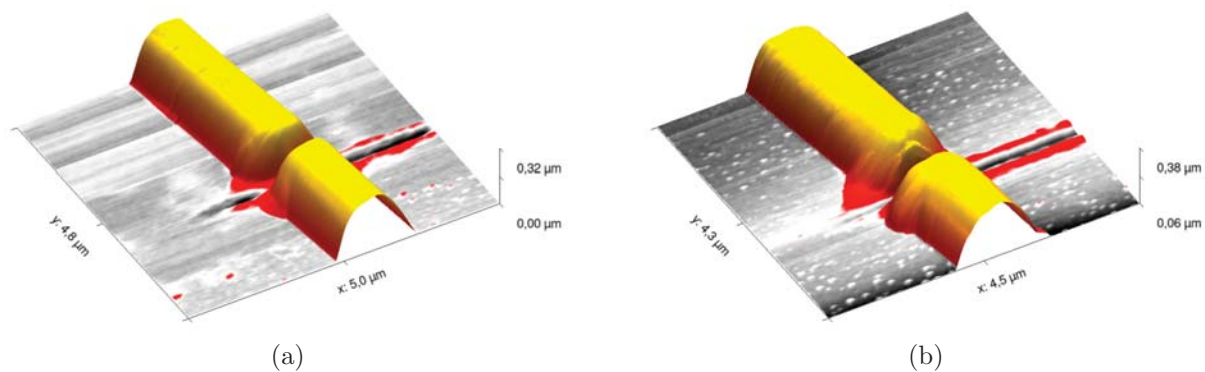
Figure 3.8.: Contact mode AFM images of the crystal shown in figure 3.6. The images were taken at the two positions marked in figure 3.6b. a) was taken at the same position as figure 3.7 after overshooting, b) was taken in a similar way a few µm to the top.

A second crystal on SiO_2 was cut with the same method. A stable image was achieved with $I_{gain} = 80\,Hz$, $P_{gain} = 0.002$, $V_{setpoint} = 0.5\,V$ and a line rate of $1\,Hz$, corresponding to a scan speed of $3\,\mu m/s$. In this case, overshooting started when increasing the gain to $P_{gain} = 0.012$. The difference between the gains for different crystals can be explained with their height. The crystal shown in figure 3.9 has a height of about $550\,nm$. The first crystal shown in this section is about $300\,nm$ high, thus an overshoot needs a higher gain ($P_{gain} = 0.014$).

As one can see in figure 3.9d, the material cut out is deposited next to the crystal. As well, the crystal was not cut through all the way down to the substrate. In the corresponding optical microscopy images, one can see that remaining link between the two parts can not be crystalline anymore, as it does not exhibit birefringence anymore. The gap showing no birefringence in optical microscopy as is much larger than the cut, which is only in the order of $100\,nm$ as one can see from AFM investigation. Thus we conclude, that the hammering with the tip destroyed the crystalline order in a large volume (the hole crystal volume along a few μm).
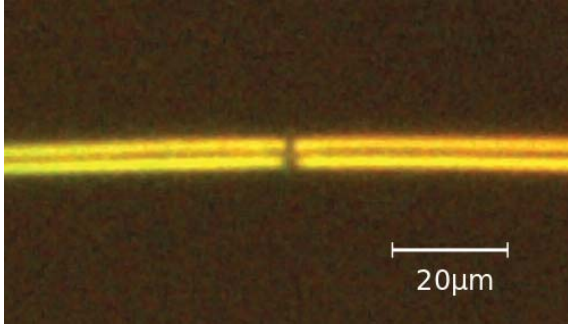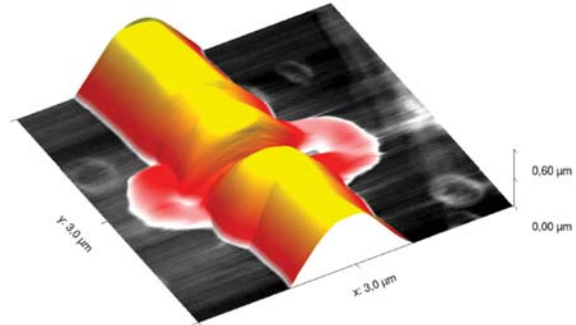
(a) Optical microscopy image with crosspolarisers after measurement, where the cut is clearly visible.
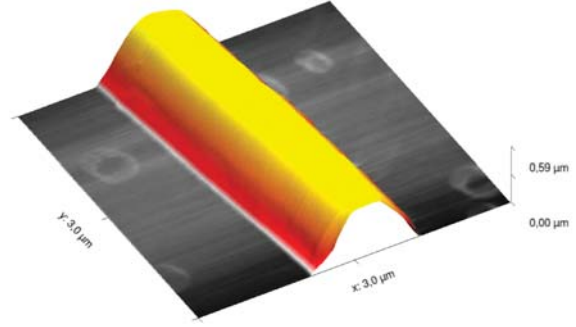
(b) AFM image done before overshooting.
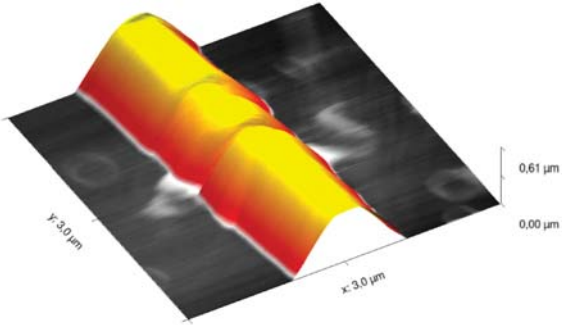
(c) AFM image taken after a single short overshooting scan (using 5 scan lines) in the central region. This image was taken at the same position as figure 3.9b.

(d) Another scan at the same position after a couple more overshooting scans, again performed in the central region. Amorphous material was displaced to both sides of the cut.

Figure 3.9.: Optical microscopy and AFM images illustrating the gradual cutting of a crystal.

In order to estimate the energy transferred from the tip to the sample we suggest a simple model. When the tip comes back into contact after the first overshoot, its energy is given by the sum of the harmonic potential of the cantilever spring and the kinetic energy added by the piezo element. We assume that the cantilever with spring constant k_{can}, is elongated after overshooting to a distance x_{max}. Therefore the potential energy is given by $V_{har} = kx^2$, which will be transferred to kinetic energy when hitting the crystal. The maximum distance of overshooting x_{max} largely depends on the step height causing the overshoot, it will be in the same order of magnitude, with the step height itself as upper limit. For this estimation we approximate x_{max} with the crystal step size. In addition to the energy coming through the cantilever spring, the piezo is still moving downwards at the moment when the tip hits the crystal, thus adding its kinetic energy E_{kin}.

$$E_{\text{tot}} = V_{\text{har}} + E_{\text{kin}} \tag{3.1}$$

$$= k_{\text{can}} x_{\text{max}}^2 + m_{\text{sys}} v_{\text{pzo}}^2 \tag{3.2}$$

The system mass m_{sys} can be estimated as the effective mass of the harmonic oscillator. This is given by

$$m_{\text{sys}} = \left(\frac{1}{2\pi f_0} \right)^2 k_{\text{can}} \tag{3.3}$$

with the resonance frequency f_0.

$$E_{\text{tot}} = k_{\text{can}} x_{\text{max}}^2 + \frac{k_{\text{can}} v_{\text{pzo}}^2}{4\pi^2 f_0^2} \tag{3.4}$$

When using the following values for the estimation

$$x_{\text{max}} = 1 \, \mu\text{m} \tag{3.5}$$

$$k_{\text{can}} = 0.2 \, \frac{\text{N}}{\text{m}} \tag{3.6}$$

$$f_0 = 100 \, \text{kHz} \tag{3.7}$$

$$v_{\text{pzo}} = 1 \, \frac{\text{mm}}{\text{s}} \tag{3.8}$$

one finds the following estimates for the energies

$$V_{\text{har}} = 2 \times 10^{-13} \, \text{J} \tag{3.9}$$

$$E_{\text{kin}} = 5 \times 10^{-19} \, \text{J} \tag{3.10}$$

Thus, the kinetic energy given by the piezo scanner movement E_{kin} can be neglected. These values give an upper bound to the deposited energy, since the collision may not be fully inelastic. Estimating the binding energy for a π-stacked crystal to be about $10 \, \text{kJ/mol}$, a single hit with the tip could break the crystal structure of up to 10 million molecules at once.

3.2.4. Cutting in non-contact mode

The idea of hammering with the tip can easily be transferred to non-contact mode. Since the tip already oscillates in this mode in a controlled fashion, we expect that a huge increase in interaction force between tip and sample will yield similar results. Besides, we found a better controllable technique in this adaptation. Moreover, it gives additional insight, since we could destroy only the crystalline order, leaving the molecules in place. However, this was enough to introduce a predetermined breaking point at which the crystal then broke.

Figure 3.10a and figure 3.10b show polarising microscopy images before and after such a manipulation of a crystal.

(a)	(b)
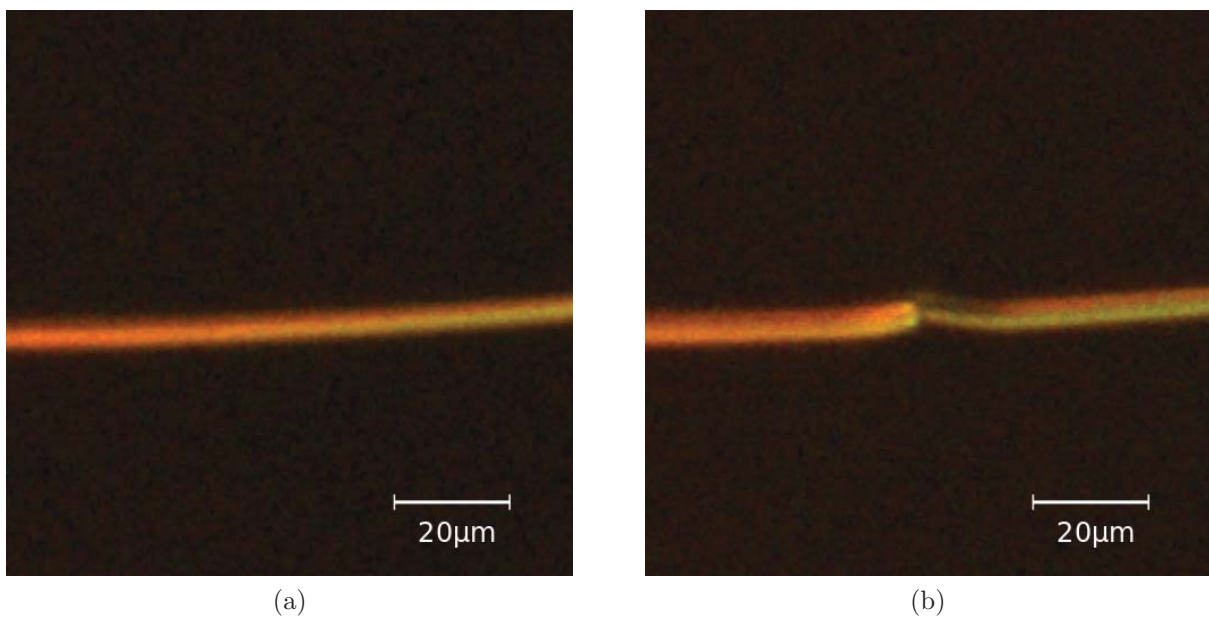
Figure 3.10.: Images of the crystal taken with polarising microscope. Picture a) was taken before and b) after measuring with non-contact mode AFM.

As in the previous section we started by scanning the crystal (figure 3.11a), which was deposited on SiO_2 out of solution ($c = 0.01\,\mathrm{mg/ml}$). Subsequently we set the tip in the middle of the scanned area and started measurement in normal scanning mode. Increasing the forces between tip and sample drastically, leads to instabilities in tip movement, and changes the crystal structure as expected. We reduced the setpoint to $0.05\,\mathrm{V}$, and, in order to stabilise the tip movement, decreased the integral gain to $I_{\mathrm{gain}} = 10\,\mathrm{Hz}$. Rescanning the same lines for several times and taking another AFM non-contact image with normal settings at the same position lead to figure 3.11b. One can clearly see that the structure was changed dramatically. Again, the crystal is not cleaved but

the molecular conformation changed. The material is amorphous after the scanning and the crystal broke at the scanned position. This can also be seen in polarising microscopy, since unordered structures appear darker when using crossed polarisers. In figure 3.10b there is a small gap in polarising microscopy, while we can see that the amorphous ends of both crystal pieces still touch each other in the AFM image (figure 3.11b) It was even possible to tilt, bend and move the crystal up to several hundred nm.

(a) (b)
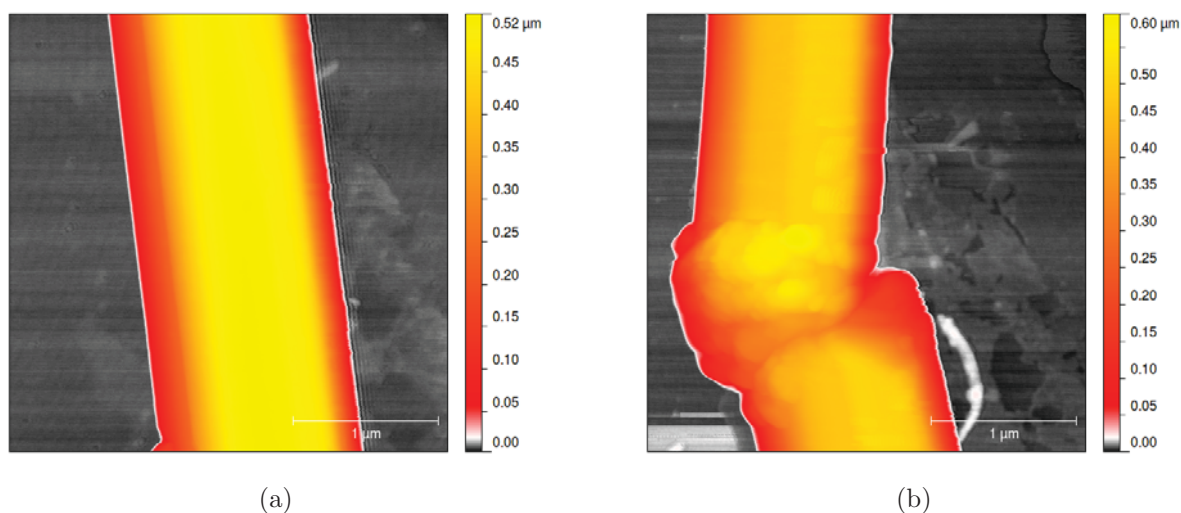
Figure 3.11.: Images of the crystal taken with non-contact AFM. Picture a) was taken before and b) after manipulating the crystal.

3.3. Charge transport measurements on 3TBT crystals

In order to reveal the charge transport mechanism for the 3TBT crystals, we performed measurements with C-AFM. The experiments were conducted on graphite and SiO_2 with gold lines. Exemplary, we present a measurement of a crystal lying flat on a contacted gold line on SiO_2, shown in figure 3.12. The current image shows a rather low conductivity of the crystal compared to the gold contact. The same result can be obtained from the measured I-V-spectrum. Finally, this confirms that the conductivity along the sidechain direction is very low (as expected). In addition, we conclude that the charge transport through the sidechains is dominated by electrons (i.e. the electron mobility is much higher than the hole mobility), as the I-V-spectrum is asymmetric with a much higher current for negative applied voltages.
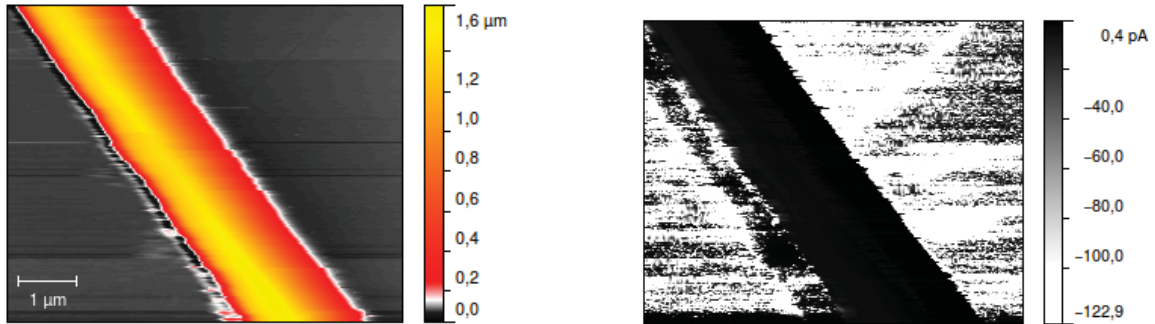
(a)

(b)
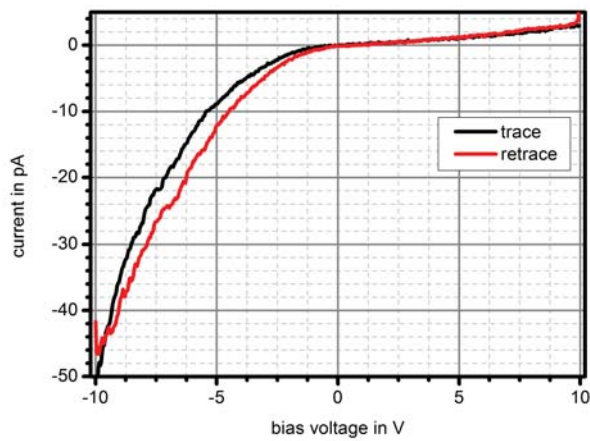
(c)

Figure 3.12.: Image of a stable crystal taken with C-AFM, the applied bias voltage was $V = 30\,\text{mV}$. Comparing the height (a) and current (b) image reveals that the conductivity of the crystal is very low. We assume that the rather low conductivity on parts of the gold substrate is due to residues of 3TBT molecules sticking to the tip, as this tip was used before when measuring a crystal that broke under measure. The I-V-spectrum taken on this crystal is shown in (c).

4. Discussion of mechanical and electronic properties

First we discuss the mechanical properties of the single crystals and what we can conclude from our measurements. In the second part of this chapter, we commit ourselves to the charge transport properties.

4.1. Defects in the crystal

Theoretically, a lower crystal quality with many defects could make the material less resistant against breaking. Thus the breaking can as well be caused by defects like dislocations and grain boundaries in the crystal structure. An assembly of such defects is invisible through optical microscopy, but may act as a predetermined breaking point when hit with the tip. Of course, proving this theory with optical microscopy and AFM only is a hard task, since the existence of such a weak zone in the crystal will cause the breaking by AFM, while it is not possible to scan at this interesting position. On the other hand, we found indication of such a reasoning shown in figure 4.1. When scanning this crystal, which was deposited on SiO_2, the crystal did not break in the beginning, but the scan was unstable. Trying to adopt the parameters to stabilise the measurement did not improve the scan.

After scanning for a few minutes, approximately $1\,\mu m$ from the beginning of the scan, suddenly the measurement was stable again, without any parameter change during this time. We suggest that the crystal was easily bent perpendicular to the long axis of the crystal, since the scan was close to a weak zone in the crystal allowing such a movement, which was observed indirectly as instability in tip movement. When reaching closer to this weak spot, the forces acting were increasing, until the weak zone ruptured along the defect lines. This happened approximately $1\,\mu m$ from the beginning of the scan, but we assume that the weak zone in the crystal was outside the scanning area, so that we could not image the broken part in this scan. Figure 4.2 shows optical microscopy images before and after measurement.
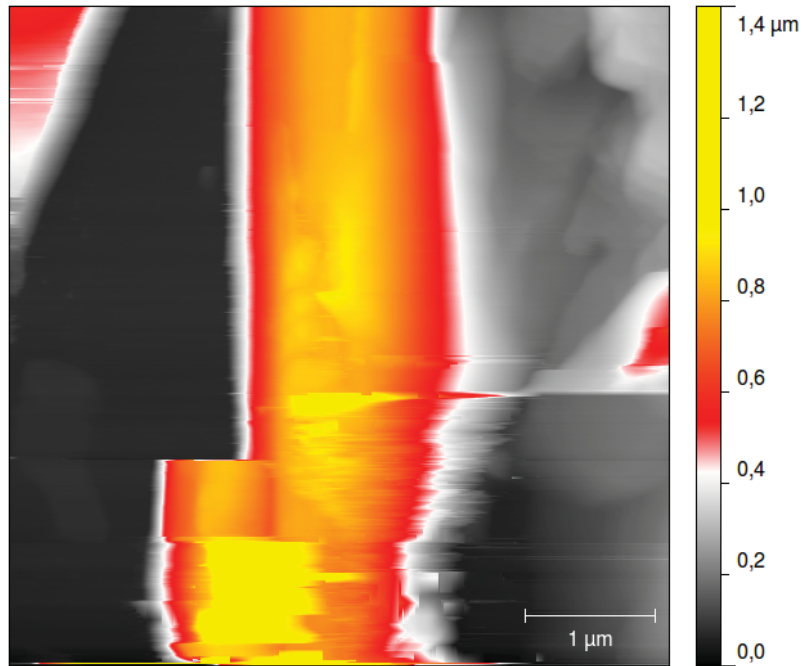
Figure 4.1.

In these images one can easily see a birefringent but at the large scale unstructured object surrounding the thick end of the crystal, around the position where it finally broke. Since its intensity is much lower than the intensity of the crystalline part, we suggest this is a semi-ordered film. This could be caused by rests of solvent that evaporated fast, with potential effects on the quality of the crystal structure in this area. This supports the theory that there was an assembly of defects causing a weak zone in this area.

Besides imaging such a weak zone directly, one can also create one by mechanical interaction. This has been shown for contact and non-contact mode scans. While the overshooting method in contact mode splits the crystal in two separated parts, it is possible to control the process in non-contact mode. When acting on the crystal in non-contact mode, the crystalline structure first changes its conformation visibly. When one tries to measure such a spot then, it directly breaks at this position. We assume that hitting the crystal with the tip introduces many grain boundaries and may even destroy the crystalline order of many molecules.

As we observed breaking of the crystal both with an upright tip and with an inclined tip against the crystal, this can not be the only reason for breaking. Breaking of the crystal after switching the tip from upright to inclined is not clear proof of this theory either. In fact, it is still consistent with the theory of the weak zone, since approaching
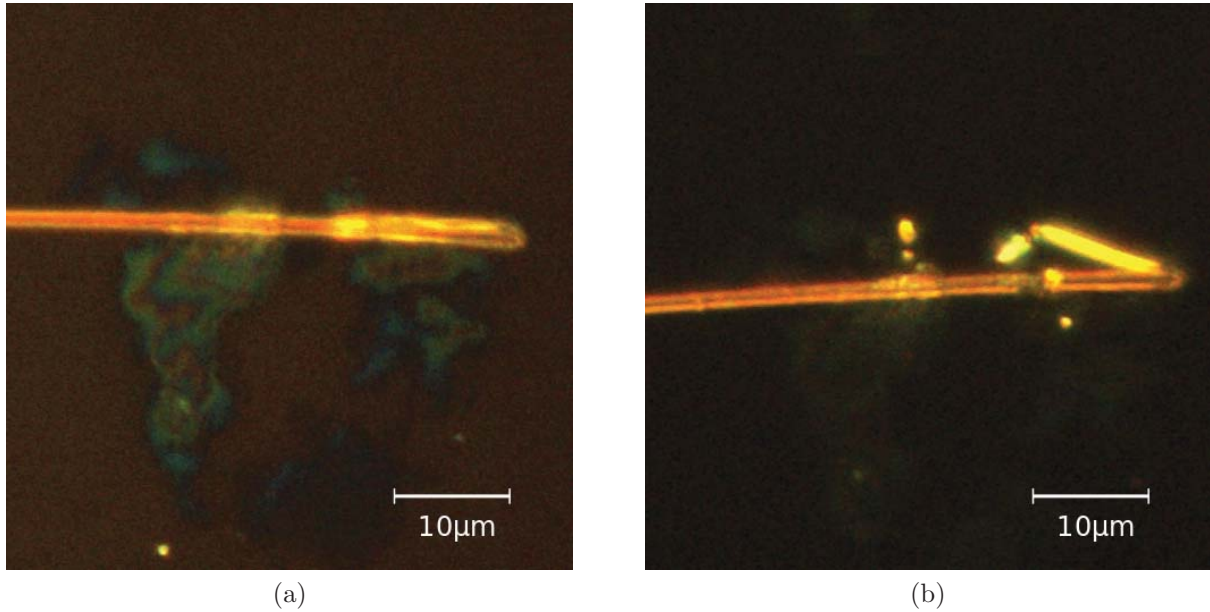
Figure 4.2.

again after changing the scanning direction may not result in the exact same position. Thus we may have scanned closer to the weak zone with inclined tip than we did with the upright tip before, therefore acting with a higher force on the weak zone and breaking the crystal.

Eventually we can conclude that there is much evidence for defects playing a major role in crystal breaking. We can also force the crystal to change its conformation at a specific position and break it at any desired point.

4.2. Charge transport measurements

The charge transport perpendicular to the substrate was measured in agreement with the orientation known from polarising microscopy, finding the transport along the sidechain direction dominated by electrons. Since the mobility along the π-stacking direction is expected to be much higher, in contrary to the measurements performed on oligothiophene crystals [9], 3TBT needles do not allow a conductivity measurement along the π-stacking direction, as the highly conducting TBT-backbone is oriented parallel to the surface. Nevertheless, we established C-AFM in UHV and gained insight into the mechanical properties of 3TBT crystals, providing the basis for future research.

5. Summary and outlook

5.1. Summary

In summary, we have investigated the mechanical and electronic properties of single-crystals consisting of 3TBT molecules, belonging to a newly synthesised family of organic semiconducting oligomers. The needle-shaped crystals may break easily during scanning with C-AFM. The orientation of the molecules in the crystal can be identified with polarising microscopy (see figure 5.1).
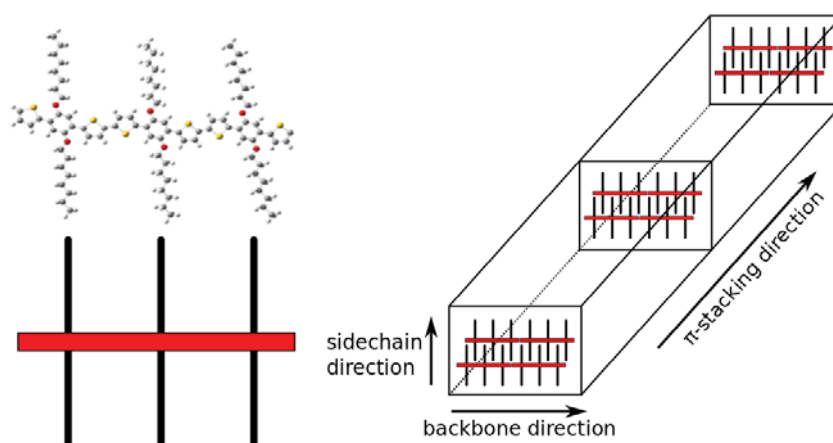

Figure 5.1.: The orientation of the molecules in the crystal.

We found two comparable methods to cut the crystals at precisely defined spots, using either contact or non-contact mode. In addition, it is possible to move the crystal parts in an undirected manner over the surface. In principle we understand the breaking mechanism as being caused by mechanically weak zones induced by a high concentration of crystal defects. Thus, the breaking of the crystals can not be avoided completely. On the other hand, we were able to show that we can introduce crystal defects through interactions with the AFM tip. We found that such defects can only be introduced through vertical forces acting along the sidechain direction, but not through horizontal interactions acting along the backbone direction. Thus, defects can be introduced through overshooting of the tip in contact mode, which may happen by accident when approaching

a crystal using too high gain values. This is counterintuitive, as one normally uses high gain values in order to avoid high (lateral) forces, when moving the tip over the edge of a crystal. But here, high vertical forces as induced by an overshoot are much more damaging, thus the intuitive starting parameters lead to an increased risk of damaging crystals.

The investigation of the electrical properties was limited by several reasons: Firstly, the breaking mechanism had to be investigated before reliable current measurements could be performed. Secondly, the frequent breaking of the crystals forced us to fall back onto AFM devices which were easier to handle than the established UHV system. Lastly, the molecular orientation in the available crystals was not advantageous for C-AFM measurements. In principle, charge transport properties can be measured in two directions along single-crystals, which exhibit anisotropic charge transport. One perpendicular to the substrate, as can be seen easily, and the other along the crystal axis, as long as the conductivity perpendicular to the substrate is much higher than along the crystal axis. As the orientation of the backbone of the molecules, i.e. the direction along we expect very high conductivity, is parallel to the substrate, only the trivial direction perpendicular to the substrate was available. Therefore we were limited to charge transport measurements along the sidechains of the molecules. Nevertheless, we showed that charge transport and exceedingly hole transport was suppressed along the direction of the sidechains.

5.2. Outlook

Finally, we close this thesis with an outlook and a discussion of the open questions.

In principle, we should prove the assumption of zones with high defect concentration in some of the crystals, as it was suggested due to the mechanical instabilities. This could be done for example with transmission electron microscopy.

Future studies will mainly aim at the possibilities to measure the conductivity along the other molecular axes, as we were limited to conductivity measurements along the sidechains in this study. In principle, two fundamentally different approaches are promising. Changing the orientation of the molecules with respect to the surface plane on the one side, and applying direct contacts at the crystals as they are. There are many different possibilities to realise both approaches.

Contacts can be applied with liquid metals or emulsions with conducting nanoparticles, attached to either the ends or to both sides of the crystals. As well, graphene flakes may establish such a contact. Maybe the most simple approach to measure the conductivity along the π-stacking direction is to deposit the crystals onto a SiO_2-sample with separately

contacted but nearby gold lines. Such a sample was already completed successfully in the scope of this thesis, but measurements were not done due to time restrictions. For every crystal that connects two gold lines, the conductivity along the long axis can easily measured by comparing the current on the contacted gold line with the current on the not contacted one. AFM can directly provide the cross section and distance between the gold contacts measured along the crystals. Even though all approaches with direct contacts are relatively fast and easy to applicate, they again introduce contact effects, while avoiding these was the main reason for using C-AFM. However, such measurements could give a quick insight in the anisotropy of the charge transport.

In order to circumvent these contact effects, crystallisation out of melt will be a hot topic. By tuning the interactions between TBT molecules and the substrate, we will grow crystals with different molecular orientations with respect to the sample surface. Growing crystals with a backbone orientation perpendicular to the surface plain will enable us to measure the conductivity along the backbone. In addition, if the current flow is as anisotropic as expected, this configuration will also allow measurements along the π-stacking direction, analogue to the measurements conducted by Wael Hourani on oligothiophene single-crystals [9]. In principle, crystal growth with π-stacking perpendicular to the surface is also an option. Another idea is to grow mexican hat shaped structures, on which one could easily measure the dependence between the current and the crystal height. Mexican hat structures are grown out of a droplet of melt. When such a droplet is wetting the surface, a large monolayer surrounds the droplet. The monolayer is seen as the rim of the hat, the droplet being the hats main part. Crystallising such a droplet on top of its own monolayer can change the orientation of the molecules as desired, depending of course on the various interactions with the specific substrate. The hat like shape forms stacked monolayers when crystallised. With the high resolution of AFM we could then specify the height and the exact number of layers, through which the current flows.

Since mexican hat structures can be grown much larger than needle shaped crystals, they could be used in the UHV AFM. There they could be seen without effort in the optical system from outside the UHV chamber, allowing measurements of the temperature dependence.

Acknowledgment

A. Appendix

A.1. Bulge lines on graphite

In order to prove that triangular structures do not consist out of 3TBT, we searched for bulge lines on a graphite sample, without depositing 3TBT crystals on it. The measurements were taken in non-contact mode with the AFM from JPK. The shapes of the bulge lines are quite similar to the crystal structure (figure A.1a), except for the more pointed height profile (figure A.1b).
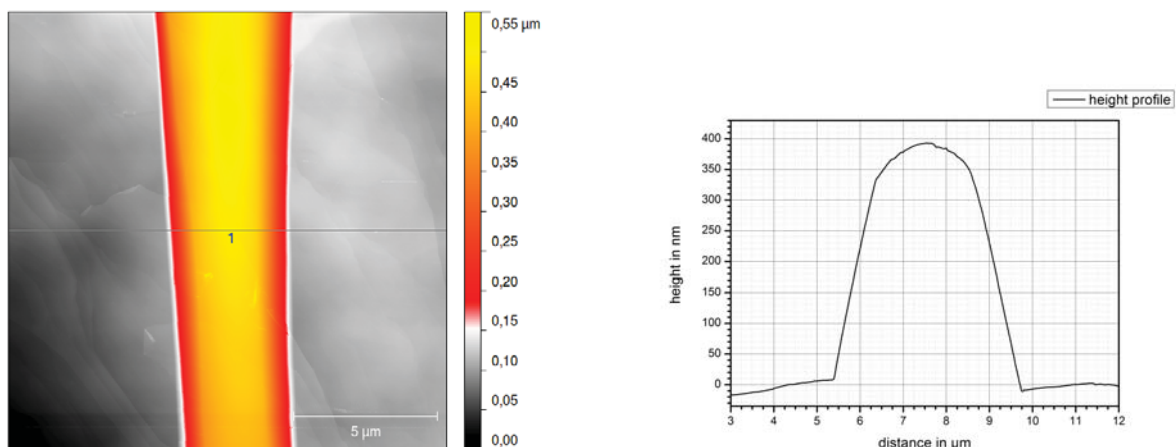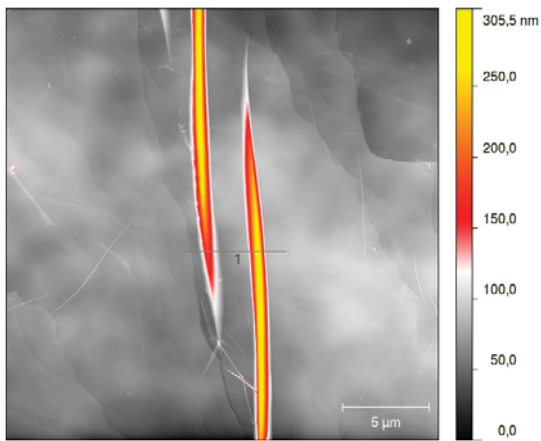

(a) Non-contact AFM image from a bulge line on clean graphite.

(b) Corresponding height profile.

Figure A.1.

Images with a larger scale (see figure A.2a) reveal different shapes at the ends, having the same shape but with decreasing height until the bulge line vanishes. In contrast, crystals have a relatively sharp, amorphous structured end. However, the bulge lines correspond clearly to the objects we misinterpreted as triangular crystals.

(a) Large scale non-contact AFM image of two bulge lines on clean graphite.
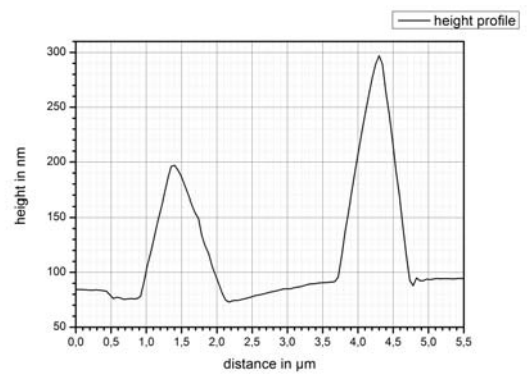
(b) Corresponding height profiles.

Figure A.2.

Bibliography

[1] Serap Günes, Helmut Neugebauer, and Niyazi Serdar Sariciftci. "Conjugated Polymer-Based Organic Solar Cells". In: *Chemical Reviews* 107 (2007).

[2] Yutaka Wakayama, Ryoma Hayakawa, and Hoon-Seok Seo. "Recent progress in photoactive organic field-effect transistors". In: *Science and Technology of Advanced Materials* 15.2 (2014).

[3] R. W. I. Boer et al. "Organic single-crystal field-effect transistors". In: *Physica status solidi* 201 (2004).

[4] Henning Sirringhaus. "25th Anniversary Article: Organic Field-Effect Transistors: The Path Beyond Amorphous Silicon". In: *Advanced Materials* 26 (2014).

[5] Chao Tang et al. "Study of carrier mobility of N,N'-diphenyl-N,N'bis(1,1'-biphenyl)-4,4'-diamine (NPB) by transmission line model of impedance spectroscopy". In: *Thin Solid Films* 542 (2013).

[6] S. Yoshimoto et al. "Independently driven four-probe method for local electrical characteristics in organic thin-film transistors under controlled channel potential". In: *Review of Scientific Instruments* 82.093902 (2011).

[7] C. Y. H. Chan et al. "Achieving time-of-flight mobilities for amorphous organic semiconductors in a thin film transistor configuration". In: *Organic Electronics* 14 (2013).

[8] B. D. Chapman et al. "Dislocations and grain boundaries in semiconducting rubrene single-crystals". In: *Journal of Crystal Growth* 290 (2006).

[9] Wael Hourani et al. "Anisotropic charge transport in large single crystals of π-conjugated organic molecules". In: *Nanoscale* (2014).

[10] G. Binnig, C. F. Quate, and Ch. Gerber. "Atomic Force Microscope". In: *Physical review letters* 56.9 (1986).

[11] G. Binnig et al. "Surface Studies by Scanning Tunneling Microscopy". In: *Physical Review Letters* 49.1 (1982).

[12] Franz J. Giessibl. "AFM's path to atomic resolution". In: *Materials Today* 8 (2005).

[13] Peter Eaton and Paul West. *Atomic Force Microscopy*. OUP Oxford.

[14] J. P. Cleveland et al. "Energy dissipation in tapping-mode atomic force microscopy". In: *Applied Physics Letters* 72.20 (1998).

[15] Günter Reiter et al. "Direct Visualization of Random Crystallization and Melting in Arrays of Nanometer-Size Polymer Crystals". In: *Physical Review Letters* 87.22 (2001).

[16] *MultiMode 8*. online accessible at http://www.bruker.com/products/surface-analysis/atomic-force-microscopy/multimode-8/technical-details.html.

[17] S. C. Tse, S. W. Tsang, and S. K. So. "Polymeric conducting anode for small organic transporting molecules in dark injection experiments". In: *Journal of Apllied Physics* 100.063708 (2006).

[18] Tino Zimmerling and Bertram Batlogg. "Improving charge injection in high-mobility rubrene crystals: From contact-limited to channel-dominated transistors". In: *Jounral of Applied Physics* (2014).

[19] R. G. Kepler. "Charge Carrier Production and Mobility in Anthracene Crystals". In: *Physical Review* 119.4 (1960).

[20] R. Dost, A. Das, and M. Grell. "Time-of-flight mobility measurements in organic field-effect transistors". In: *Journal of Applied Physics* 104.084519 (2008).

[21] R. A. Laudise et al. "Physical vapor growth of organic semiconductors". In: *Journal of Crystal Growth* (1998).

[22] Xionghui Zeng et al. "Morphology and fluorescence spectra of rubrene single crystals grown by physical vapor transport". In: *Applied Surface Science* (2007).

[23] *The effect of temperature and gas flow on the physical vapour growth of mm-scale rubrene crystals for organic FETs*. 2008.

[24] Ch. Kloc et al. "Physical vapor growth of centimeter-sized crystals of α-hexathiophene". In: *Journal of Crystal Growth* (1998).

[25] Shuhong Liu et al. "Controlled Deposition of Crystalline Organic Semiconductors for Field-Effect-Transistor Applications". In: *Advanced Materials* (2009).

[26] Nguyen T. K. Thanh, Maclean N., and Mahiddine S. "Mechanisms of Nucleation and Growth of Nanoparticles in Solution". In: *Chemical Reviews* (2014).

[27] Rongjin Li et al. "Micro- and Nanocrystals of Organic Semiconductors". In: *Accounts of chemical research* 43.4 (2010).

[28] K. Taguchi et al. "Growth shape of isotactic polystyrene crystals in thin films". In: *Polymer* 42 (2001).

[29] H. Zhang et al. "Correlating Polymer Crystals via Self-Induced Nucleation". In: *Physical Review Letters* 112.237801 (2014).

[30] Richard Phillips Feynman, Robert Benjamin Leighton, and Matthew Sands. *The Feynman Lectures on Physics (online edition)*. Ed. by Michael A. Gottlieb and Rudolf Pfeiffer. California Institute of Technology, 2010.

[31] P. Hermet et al. "Far-infrared spectroscopy investigation of sulfur-oxygen interactions in π-conjugated oligomers". In: *Chemical Physics Letters* (2012).

[32] Roozbeh Shokri et al. "Generating Long Supramolecular Pathways with a Continuous Density of States by Physically Linking Conjugated Molecules via Their End Groups". In: *Journal of the american chemical society* (2013).

[33] J. Vrijmoeth et al. "Single crystallites in "planar polycrystalline" oligothiophene films: Determination of orientation and thickness by polarization microscopy". In: *Journal of Applied Physics* 83.7 (1997).